Formation of condensable organic vapors from anthropogenic and biogenic VOCs is strongly perturbed by NO$_x$ in eastern China

Yuliang Liu[1,2], Wei Nie[1,2*], Yuanyuan Li[1,2], Dafeng Ge[1,2], Chong Liu[1,2], Zhengning Xu[1,2,5], Liangduo Chen[1,2], Tianyi Wang[1,2,10], Lei Wang[1,2], Peng Sun[1,2], Ximeng Qi[1,2], Jiaping Wang[1,2], Zheng Xu[1,2], Jian Yuan[1,2], Chao Yan[3], Yanjun Zhang[3,9], Dandan Huang[4], Zhe Wang[6], Neil M. Donahue[7], Douglas Worsnop[8], Xuguang Chi[1,2], Mikael Ehn[3], and Aijun Ding[1,2]

[1] Joint International Research Laboratory of Atmospheric and Earth System Sciences, School of Atmospheric Sciences, Nanjing University, Nanjing, Jiangsu Province, China

[2] Collaborative Innovation Center of Climate Change, Jiangsu Province, China

[3] Institute for Atmospheric and Earth System Research/Physics, Faculty of Science, University of Helsinki, Helsinki, Finland

[4] State Environmental Protection Key Laboratory of Formation and Prevention of Urban Air Pollution Complex, Shanghai Academy of Environmental Sciences, Shanghai, China

[5] College of Environmental & Resource Sciences, Zhejiang University, Zhejiang, China

[6] Department of Civil and Environmental Engineering, the Hong Kong Polytechnic University, Hong Kong SAR

[7] Center for Atmospheric Particle Studies, Carnegie Mellon University, Pittsburgh, PA, USA

[8] Center for Aerosol and Cloud Chemistry, Aerodyne Research Inc., Billerica, MA, USA

[9] Univ. Lyon, Université Claude Bernard Lyon 1, CNRS, IRCELYON, 69626, Villeurbanne, France

[10] Meteorological Service Center of Hubei Province, Wuhan, 430074

Abstract

Oxygenated organic molecules (OOMs) are the crucial intermediates linking volatile organic compounds (VOCs) to secondary organic aerosol (SOA) in the atmosphere, but comprehensive understandings of the characteristics of OOMs and their formations from VOCs are still missing. Ambient observations of OOMs using recently developed mass spectrometry techniques are still limited, especially in polluted urban atmosphere where VOCs and oxidants are extremely variable and complex. Here, we investigate OOMs, measured by a nitrate-ion-based chemical ionization mass spectrometer at Nanjing in eastern China, through performing positive matrix factorization on binned mass spectra (binPMF). The binPMF analysis reveals three factors about anthropogenic VOCs (AVOCs) daytime chemistry, three isoprene-related factors, three factors about biogenic VOCs (BVOCs) nighttime chemistry, and three factors about nitrated phenols. All factors are influenced by NO$_x$ in different ways and to different extents. Over 1000 non-nitro molecules have been identified and then reconstructed from the selected

solution of binPMF, and about 72% of the total signals are contributed by nitrogen-containing OOMs, mostly regarded as organic nitrates formed through peroxy radicals terminated by nitric oxide or nitrate-radical-initiated oxidations. Moreover, multi-nitrates account for about 24% of the total signals, indicating the significant presence of multiple generations, especially for isoprene (e.g., $C_5H_{10}O_8N_2$ and $C_5H_9O_{10}N_3$). Additionally, the distribution of OOMs concentration on carbon number confirm their precursors driven by AVOCs mixed with enhanced BVOCs during summer. Our results highlight the decisive role of NO_x on OOMs formation in densely populated areas, and encourage more studies on the dramatic interactions between anthropogenic and biogenic emissions.

1 Introduction

Secondary organic aerosol (SOA), as an important and complex component of submicron particles (Zhang et al., 2007;Jimenez et al., 2009;Huang et al., 2014), is fully involved in affecting climate (Intergovernmental Panel on Climate, 2014) and causing health risks (Nel, 2005;Lim et al., 2012). Volatile organic compounds (VOCs) are ubiquitous in the atmosphere and are recognized as main precursors of SOA (Hallquist et al., 2009;Ziemann and Atkinson, 2012). However, the missing intermediate processes from VOCs to SOA are yet to be elucidated (Hallquist et al., 2009;Ehn et al., 2014).

Benefitting from the state-of-the-art measurement technics (Bertram et al., 2011;Jokinen et al., 2012;Lee et al., 2014), many previously unreported oxygenated organic molecules (OOMs), as intermediates from VOCs to SOA (Ziemann and Atkinson, 2012), have been discovered. Among OOMs, highly oxygenated organic molecules (HOMs), first observed in the gas phase at a boreal forest site (Ehn et al., 2010;Ehn et al., 2012) and have been reviewed by Bianchi et al. (2019), are so functionalized and low volatile that they can participate at the beginning of new particle formation (NPF) by stabilizing sulfuric acid (Kulmala et al., 2013;Riccobono et al., 2014) or through clustering alone (Kirkby et al., 2016;Bianchi et al., 2016), and condense on existing particles to be responsible for a large fraction of SOA (Ehn et al., 2014). In addition to conventional VOCs-to-OOMs mechanisms summarized in the Master Chemical Mechanism (MCM) (http://mcm.york.ac.uk/, last access: 09 February 2021), recent studies have proposed new pathways, such as autoxidation (Crounse et al., 2013;Jokinen et al., 2014) and multigenerational oxidation (Rollins et al., 2012;Wang et al., 2020b), to form condensable vapors by adding oxygen atoms efficiently. The productions of OOMs, especially HOMs, from precursors such as monoterpenes (Ehn et al., 2014;Jokinen et al., 2015;Kirkby et al., 2016;Berndt et al., 2016), sesquiterpenes (Richters et al., 2016), isoprene (Jokinen et al., 2015;Zhao et al., 2020) , aromatics (Wang et al., 2017;Molteni et al., 2018;Garmash et al., 2020), and alkanes (Wang et al., 2021) have been investigated in laboratories by using the chemical ionization atmospheric pressure interface time-of-flight mass spectrometer with nitrate reagent ions (nitrate CI-APi-TOF).

84　New insights and a general understanding about OOMs have been attained, yet many
85　critical details about OOMs formation and properties need to be addressed. First, the
86　current kinetic descriptions of OOMs obtained from experiments are still limited, such
87　as the lack of individual H-shift rates for autoxidation and of reaction rates of multi-
88　generational products with oxidants. Furthermore, the complexity of the real
89　atmosphere makes it more difficult to apply experimental results to ambient
90　environments. The precursors compete for oxidants and vice versa, and their products
91　will interact mechanistically in mixtures of atmospheric vapors (McFiggans et al.,
92　2019;Heinritzi et al., 2020). However, in the laboratory we usually study simple
93　systems with a single precursor and a single oxidant. Moreover, most experiments are
94　carried out for environments dominated by biogenic VOCs (BVOCs), while
95　anthropogenic emissions receive less attention. In addition to classic anthropogenic
96　VOCs (AVOCs), large amounts of primary emissions of oxygenated VOCs are also
97　present in urban areas (Karl et al., 2018). The effect of NO_x on OOMs is another key
98　issue. NO_x can terminate peroxy radicals (RO_2), outcompeting autoxidation
99　propagation reactions and other bimolecular reactions ($RO_2 + RO_2$, $RO_2 + HO_2$), and
100　change the products distribution, and consequently, size-dependently modulate the
101　growth rates of organic aerosol particles (Yan et al., 2020). Additionally, NO_x
102　contributes non-linearly to atmospheric oxidants, which also influence the productions
103　of OOMs (Pye et al., 2019). It is anticipated that NO_x plays a varied role in the
104　formations of OOMs as well as SOA in different environments.
105
106　Therefore, more extensive OOMs observations are needed to validate the atmospheric
107　implications of experiments, to couple with the global or regional model, and finally to
108　comprehensively understand the fate of OOMs in the atmosphere. Until now, only a
109　few ambient observations of OOMs using nitrate CI-APi-TOF have been reported
110　(Bianchi et al., 2019), and almost all of them focus on rural or forested or remote
111　atmospheres (Yan et al., 2016;Massoli et al., 2018;Zhang et al., 2020;Beck et al., 2021).
112
113　The Yangtze River delta (YRD) is one of the most developed regions in eastern China.
114　Fine particulate matter, with an aerodynamic diameter smaller than 2.5 μm ($PM_{2.5}$), has
115　been significantly reduced in eastern China after the implementation of "Action Plan
116　for Air Pollution Prevention and Control" since 2013 (Ding et al., 2019), while
117　(secondary) organic aerosol are still much more abundant than in clean areas (Zhang et
118　al., 2017;Sun et al., 2020). Here we investigated condensable oxygenated organic
119　vapors observed by nitrate CI-APi-TOF in August-September 2019 at the Station for
120　Observing Regional Processes and the Earth System (SORPES) in the western part of
121　the YRD, an anthropogenic-emissions-dominated environment (Fu et al., 2013;Xu et
122　al., 2017) mixed with enhanced biogenic emissions during summer (Wang et al.,
123　2020a;Xu et al., 2021). A variety of oxidants (Liu et al., 2019;Li et al., 2020;Xia et al.,
124　2020) with numerous precursors (VOCs) suggest very complicated atmospheric
125　oxidation processes and thousands of products (OOMs). Thereby, positive matrix
126　factorization (PMF) (Paatero and Tapper, 1994) was applied to time-resolved mass
127　spectra which had been pre-divided into small bins (binPMF, Zhang et al., 2019), to

128 separate various sources or processes of OOMs. Combined with summarizing the
129 ensemble chemical characteristics of OOMs, some interesting inspirations about the
130 conversion of VOCs to OOMs were obtained.
131
132 **2 Methodology**
133
134 **2.1 Study site**
135
136 The SORPES station (32°07′14″ N, 118°57′10″ E; 62 m a.s.l.) is located at Nanjing in
137 the western part of YRD, one of the most developed regions in eastern China. Due to
138 its unique location, this site can be influenced by air masses from different source
139 regions of anthropogenic emissions, biomass burning, dust and biogenic emissions
140 (Ding et al., 2013;Ding et al., 2016). Detailed descriptions for the station can be found
141 in previous studies (Nie et al., 2015;Xie et al., 2015;Xu et al., 2018;Wang et al.,
142 2018a;Sun et al., 2018;Shen et al., 2018).
143
144 **2.2 Instrumentation**
145
146 The nitrate CI-APi-TOF (Aerodyne Research Inc. and Tofwerk AG), combining a
147 chemical ionization source (CI) and an atmospheric pressure interface time-of-flight
148 mass spectrometer (APi-TOF) equipped with a long-TOF model (LTOF) with mass
149 resolution of 8000-12000 Th/Th, was deployed to detect the ambient sulfuric acid and
150 OOMs. The ambient air was pulled into a laminar flow reactor, where the sample flow
151 (10 L min^{-1}) is surrounded by a purified airflow serving as the sheath flow (25 L min^{-1}),
152 through a stainless-steel tube (a 100 cm long, 3/4 in. diameter). Nitrate reagent ions
153 were generated in the sheath flow by exposing air-containing nitric acid to a
154 PhotoIonizer X-Ray (Model L9491, Hamamatsu, Japan). Detailed description of the
155 instrument has been described elsewhere (Junninen et al., 2010;Jokinen et al., 2012).
156 The data were acquired at 1 Hz time resolution and analyzed with a tofTools package
157 (version 6.11) based on MATLAB (Math Works Inc.). Due to the diversity and unknown
158 molecular structures of oxygenated organic compounds, standards for OOMs
159 measurable by the nitrate CI-APi-TOF are still lacking. Like other studies have done
160 (Kirkby et al., 2016;Trostl et al., 2016;Stolzenburg et al., 2018), an empirical method
161 was used to quantify the concentrations of OOMs based on the ionization kinetics
162 (pseudo first order reaction approximation) in the reaction tube of CI (Eq. 1) (Heinritzi
163 et al., 2016).
164

$$[OOM_i] = \ln\left(1 + \frac{\sum_{n=0}^{1}[OOM_i \cdot (HNO_3)_n \cdot NO_3^- + (OOM_i - H)^-]}{\sum_{n=0}^{2}[(HNO_3)_n \cdot NO_3^-]}\right) \times C \times T_i \qquad (1)$$

165

166
167 Here [OOM$_i$] is the concentration (molecules cm^{-3}) of one OOM. On the right side of
168 the equation, the numerator in the parenthesis is the detected total signals (ions/s) of
169 one OOM charged by nitrate ions in forming-adduct or deprotonated ways, the
170 denominator is the sum of all reagent ion signals (ions/s). First, a H$_2$SO$_4$-based

calibration factor C, with a value of 4.2×10^9 molecules cm^{-3}, was obtained from a calibration using H_2SO_4 (Kuerten et al., 2012) proceeding taking into account the diffusion loss in the sampling line by assuming that all detected OOMs have the same ionization efficiency as H_2SO_4. The collision frequency of HOMs with nitrate clusters is comparable to that of sulfuric acid with nitrate clusters (Ehn et al., 2014;Hyttinen et al., 2015), yet the collision frequency of some moderately oxygenated molecules with nitrate clusters is relatively slower. Therefore, calibration by this method leads to a lower limit estimate of OOMs concentrations (Ehn et al., 2014;Trostl et al., 2016), but the accurate quantification of OOMs is not the main concern of this study and the errors in the quantification of OOMs do not change our conclusions. Second, a mass dependent transmission efficiency T_i of APi-TOF was inferred in a separate experiment by depleting the reagent ions with several perfluorinated acids (Heinritzi et al., 2016).

VOCs precursors were measured by a proton transfer reaction time-of-flight mass spectrometer (PTR-ToF-MS, Ionicon Analytik, Innsbruck, Austria, TOF 1000 ultra). $PM_{2.5}$ was measured with a combined technique of light scattering photometry and beta radiation attenuation (Thermo Scientific SHARP Monitor Model 5030). The chemical compositions of $PM_{2.5}$ was determined on-line using time-of-flight aerosol chemical speciation monitor (TOF-ACSM, Aerodyne Research Inc.). PMF analysis was further used to separate the organic aerosol (OA) to primary and secondary organic aerosols (POA and SOA). The number concentrations of particles were measured by the scanning mobility particle sizer (SMPS) with nano DMA (4.0 to 63.8 nm) and long DMA (41.4 to 495.8 nm) and the aerodynamic particle sizer (APS) (0.5 to 18.0 μm). NO and NO_2 were measured using a chemiluminescence analyzer equipped with a blue-light converter (TEI, Model 42I-TL); O_3, SO_2, and CO were measured using the ultraviolet photometry, pulsed-UV fluorescence, and IR (infrared) photometry techniques (TEI, Model 49I, 43C, and 48C), respectively. Zero and span calibrations for trace gases were performed weekly during the campaign. Meteorological measurements including relative humidity (RH), wind speed, wind direction, and air temperature were recorded by Automatic Weather Station (CAMPEEL co., AG1000). $J(O^1D)$ was measured by ultra-fast CCD-detector spectrometer, UVB enhanced (Meteorologieconsult Gmbh, Germany).

2.3 Hydroxyl radical (OH) estimate

The OH concentration was calculated by applying the Eq. (2), based on the assumption that gaseous sulfuric acid is mostly produced from the oxidation of SO_2 by OH and primarily loss by condensing onto particles:

$$[OH] = \frac{[H_2SO_4]\cdot CS}{k_{OH+SO_2}\cdot[SO_2]} \tag{2}$$

Where k_{OH+SO_2} is a termolecular reaction constant for the rate-limiting step of the formation pathway of H_2SO_4 in the atmosphere (Finlayson-Pitts and Pitts, 2000), and

213 condensation sink (CS) is the loss rate of H_2SO_4 by condensation to aerosol surface.
214 The value of k_{OH+SO_2} is inferred from the IUPAC Task Group on Atmospheric
215 Chemical Kinetic Data Evaluation (https://iupac-aeris.ipsl.fr/, last access: 09 August
216 2021). The value of CS was calculated following Eq. (3) (Kulmala et al., 2012):

217

218 $$CS = 2\pi D \sum_i \beta_{m_i} d_{p_i} N_i \qquad (3)$$

219

220 Where D is the diffusion coefficient of gaseous sulfuric acid, β_m is a transition-regime
221 correction factor dependent on the Knudsen number (Fuchs and Sutugin, 1971), and
222 d_{p_i} and N_i are the diameter and number concentration of particles in size bin i.

223

224 It has been proved that $\frac{k_{OH+SO_2} \cdot [SO_2] \cdot [\cdot OH]}{CS}$ is a very reliable proxy for H_2SO_4 during the
225 day (Lu et al., 2019). The ozonolysis of alkenes can form stabilized Criegee
226 intermediates (SCIs) in addition to OH, and SCIs can also oxidize SO_2 to form H_2SO_4
227 (Mauldin Iii et al., 2012;Guo et al., 2021). A previous study on H_2SO_4 proxy in this site
228 has revealed that the reactions of SO_2 with products from the ozonolysis of alkenes
229 generate a moderate amount of nighttime sulfuric acid, with little effect on daytime
230 sulfuric acid (Yang et al., 2021). Thus, OH may be overestimated during nighttime. In
231 this study, OH was used to calculate the production rates of RO_2 during daytime (Fig.
232 4), the error of OH do not change the relative distribution of RO_2 from different
233 precursors.

234

235 **2.4 binPMF**

236

237 binPMF has been used to analyze the measured HR mass spectrometry data. Briefly,
238 the raw spectra were divided into narrow bins with a width of 0.006 Th after mass
239 calibration. The data matrix and error matrix were prepared according to the methods
240 described by Zhang et al. (2019) for the PMF model inputs (Section S2 in the
241 supplement). Different from the traditional PMF such as using unit mass resolution
242 (UMR) or HR data as input, binPMF still retains HR information as much as possible,
243 avoids the uncertainty of HR peak fitting influencing the results of PMF, and separate
244 the complex overlapping peaks for fitting. The PMF analysis in this work uses the
245 IGOR based analyzing interface SoFi (solution finder, version 6.8) and ME-2 as
246 described in (Canonaco et al., 2013). After select the PMF solution, we fitted the HR
247 peaks in each factor through toftool.

248

249 **3 Results and Discussions**

250

251 Figure 1 shows temporal variation of OOMs and related parameters at the SORPES

252 station in the northeastern suburb of Nanjing from August 02 to September 06, 2019.
253 During the observation period, 22 of 35 days had maximum hourly temperatures above
254 30 degrees Celsius, and 29 days had maximum hourly $J(O^1D)$ above 2×10^{-5} s^{-1}. High
255 temperature and solar radiation indicate strong photochemistry, producing a large
256 amount of ozone, with concentration often exceeding 80 ppb. Even at night, the
257 concentration of ozone is rarely lower than 10 ppb, resulting from the weak titration of
258 low NO. At the same time, the reaction between ozone and high concentration of NO_2
259 can provide sufficient NO_3 radicals, dominating nocturnal degradation of certain
260 volatile organic compounds (VOCs) (Wayne et al., 1991). The elevated mixing level of
261 total aromatic hydrocarbons is one of the main characteristics of the atmosphere in
262 densely populated areas, in addition to which there should be many alkanes and alkenes
263 which cannot be observed by PTR-ToF-MS (Fu et al., 2013;Xu et al., 2017). In the
264 daytime with strong photochemical reaction ($J(O^1D)> 1\times10^{-5}$ s^{-1}), we instead observed
265 higher concentrations of isoprene than total aromatics (Fig.S1(a)). The complex
266 mixtures of anthropogenic and biogenic VOCs can be oxidized through a variety of
267 pathways to produce OOMs, of which some low volatile components will condense
268 into particles, forming organic aerosol. The concentrations of OOMs with mass-to-
269 charge ratio (m/z) below 360 Th are usually higher than 10^6 molecules cm^{-3}, and some
270 can even reach up to 10^7-10^8 molecules cm^{-3}. Clustered peaks on the spectra of OOMs
271 and their clear daily variations imply a lot of chemical and physical dynamics
272 information (Fig. 1(d) and Fig.S1(b)), which is the main aspect we want to explore in
273 this work.
274
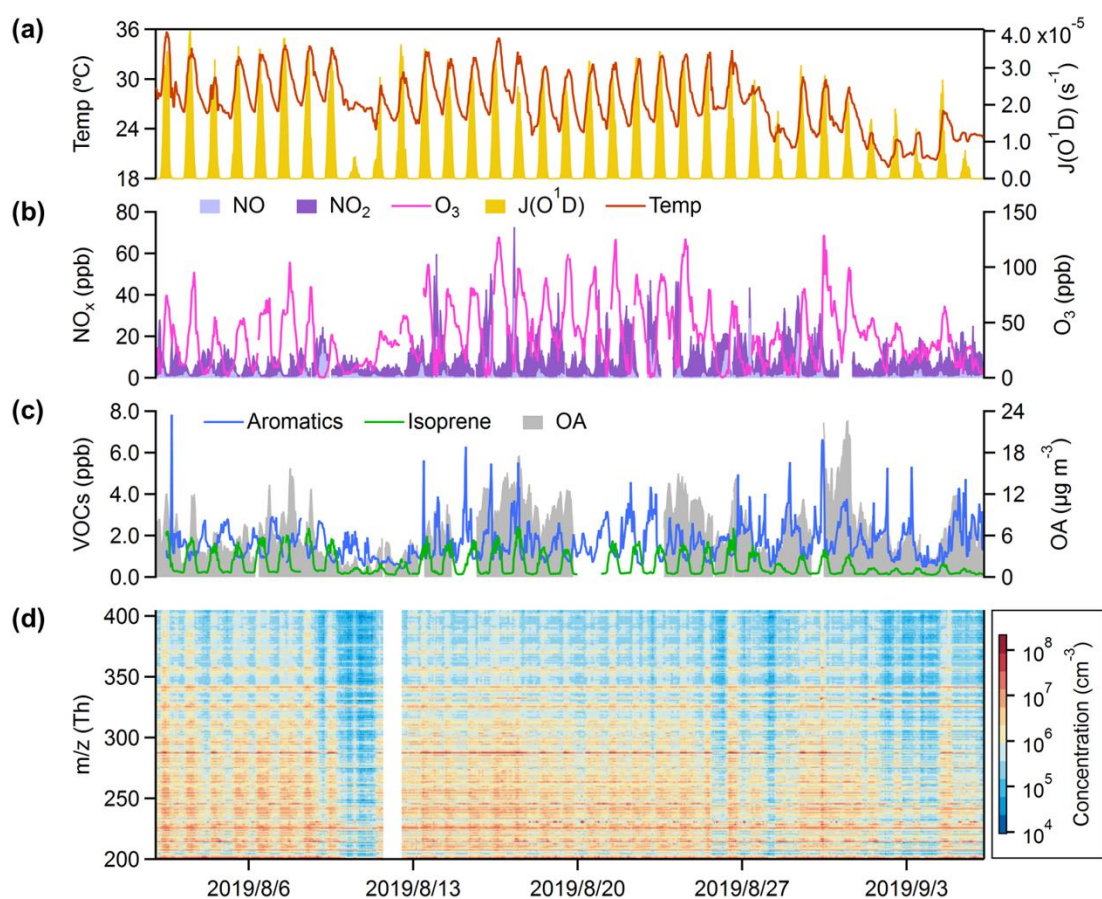
Figure 1. Overview of the observation. Time series of (a) temperature (Temp) and the photolysis frequency of O_3 (JO^1D), (b) O_3 and NO_x ($NO+NO_2$), (c) total aromatics (benzene + toluene + C_8 aromatics + C_9 aromatics + C_{10} aromatics + styrene), isoprene, and OA, and (d) mass spectra of nitrate CI-APi-TOF with m/z in the range of 202-404 Th.

The binPMF analysis was performed to characterize the sources or processes of OOMs. A 14-factor solution was selected to interpret the data set, including 3 factors about AVOCs daytime chemistry, 3 isoprene-related factors, 3 factors about BVOCs nighttime chemistry, 3 factors about nitrated phenols (NP), and 2 factors excluded from the following discussion. One of these two disregarded factors is mainly composed of fluorinated contaminations (F-contaminations), and the other is mainly a mixture of nitrated phenols and fluorinated contaminations (Mixed contaminations). When naming these factors, we prioritize the description of dominated species or their precursors, but if the precursors are complex mixtures, our naming highlights the characteristics of the chemical processes that drive certain factors. Although this may not be the optimal PMF solution, it still separates a lot of useful information. We also stress that the urban OOMs mix is unlikely to be a perfect combination of independent, unchanging factors, which is an underlying assumption in the PMF algorithm. As such, there will be no solution which is complete and perfect, but we chose a solution from which we were able to provide us with interesting insights. Details of the PMF diagnostics is provided in section S2 in the supplement (Fig. S2-S6). For the

298 convenience of discussions, we have grouped these factors based on shared
299 characteristics of certain factors.
300
301 Table 1. Summary of molecular characteristics of 9 discussed non-nitrated-phenols
302 factors. The calculation of the relevant parameters is given in section S3 in
303 the supplement. Major peaks of each factor are summarized in section S4 in
304 the supplement.

Factor	Average concentration (cm-3)	Effective formulae	MW (g mol^{-1})	OSc	O:C	N:C	DBE	$\log_{10}(C^*(\mu g\ m^{-3}))$ in 300K
Aro-OOMs	1.86E+07	$C_{9.1}H_{14.3}O_{6.1}N_{0.6}$	230.2	-0.52	0.73	0.08	2.6	-1.7
Temp-related	4.50E+07	$C_{6.8}H_{10.2}O_{6.0}N_{0.5}$	195.8	-0.02	0.95	0.08	2.5	-1.4
Aliph-OOMs	2.11E+07	$C_{7.5}H_{12.2}O_{6.7}N_{1.2}$	225.7	-0.55	0.96	0.17	1.9	0.0
Photo-related	4.77E+07	$C_{6.9}H_{11.0}O_{7.4}N_{1.2}$	228.3	-0.28	1.18	0.20	1.8	-1.1
O_x & SOA-related	2.59E+07	$C_{6.6}H_{9.8}O_{6.8}N_{1.1}$	214.2	-0.24	1.11	0.19	2.2	-0.3
Isop-OOMs	2.83E+07	$C_{5.5}H_{9.6}O_{6.9}N_{1.4}$	205.8	-0.51	1.34	0.28	0.9	1.2
BVOCs-OOMs I	1.68E+07	$C_{7.2}H_{11.5}O_{7.0}N_{1.0}$	224.1	-0.26	1.06	0.16	2.0	-1.4
BVOCs-OOMs II	9.05E+06	$C_{9.2}H_{14.6}O_{7.1}N_{0.9}$	251.3	-0.45	0.83	0.11	2.5	-2.8
BVOCs-OOMs III	1.57E+07	$C_{8.6}H_{13.7}O_{6.9}N_{1.2}$	243.3	-0.64	0.87	0.16	2.1	-0.7

305 Note: MW is the molecular weight, OSc is the carbon oxidation state, O:C is the oxygen
306 to carbon ratio, N:C is the nitrogen to carbon ratio, DBE is the double bond equivalent,
307 C* the saturation concentration and $\log_{10}(C^*)$ is the volatility.
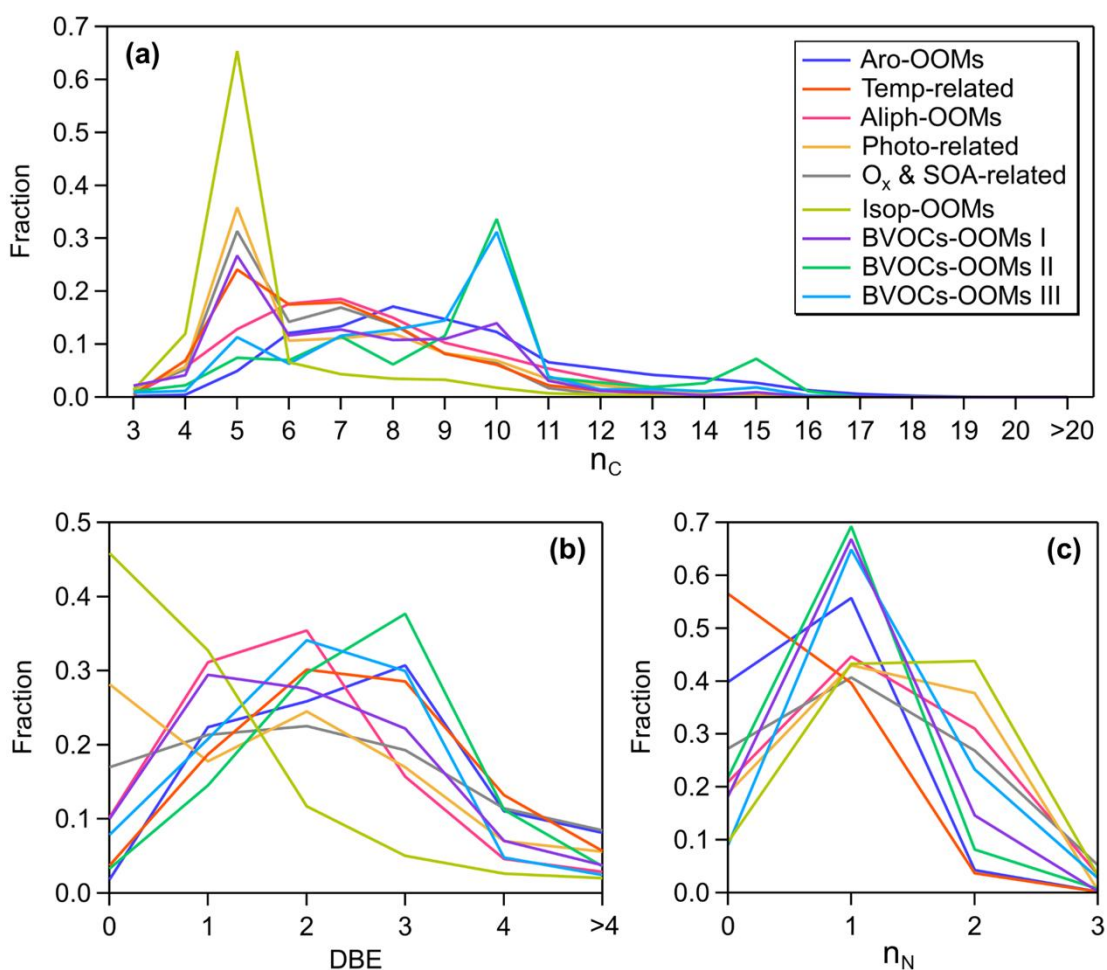308
309
310 **3.1 AVOCs daytime chemistry**
311
312 The following daytime factors are characterized by C_6-C_9 OOMs (Fig. 2(a)), considered
313 to be derived from the oxidation of anthropogenic VOCs in this urban atmosphere,
314 while we cannot completely exclude the present of BVOCs-derived OOMs, such as C_5
315 and C_{10} OOMs.
316

Figure 2. The distributions of observed non-nitro OOMs grouped by (a) the number of carbon atoms (n_C), (b) DBE, and (c) the number of nitrogen atoms (n_N) in 9 factors. Since the signals of RO_2 are very weak, RO_2 from BVOCs OOMs I and BVOCs OOMs II are excluded in (b) to keep the integer value of DBE.
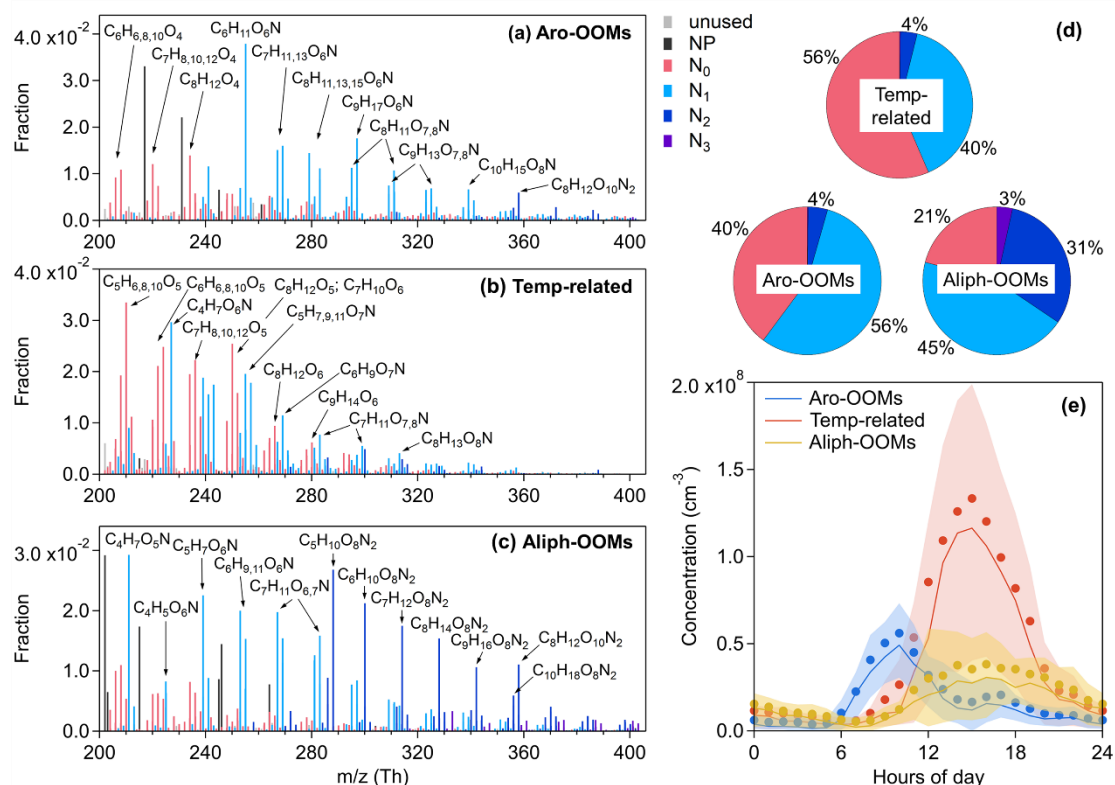
Aro-OOMs factor

The effective DBE of this factor is the largest among all factors (Table 1), with main signals come from compounds with DBE > 2 (Fig. 2(b)) and consistent with the nature of the oxidation products of aromatics (Fig. 3(a)). Combined with the correlation with the production rates of OH-initiated primary peroxy radicals (RO_2) from aromatics calculated by Eq. (4) (Fig. 4), this factor is supposedly dominated by aromatics-derived OOMs (Aro-OOMs). The Aro-OOMs factor increases from 5:00 LT with a maximum at 10:00 LT and a sub peak around 16:00 LT (Fig. 3(e)), following the diurnal variations of P_{RO_2} of C_7-C_{10} aromatics (Fig. 4(b-d)) but poorly correlated with P_{RO_2} of benzene (Fig. 4(a)). Furthermore, OOMs with 8 carbon atoms have the highest signal in this factor (Fig. 2(a)), derived from the most abundant C_8-aromatics + styrene RO_2 (Fig. 4(f)). Both of these can be explained by the fact that substituted aromatics have higher OH reactivity (Bloss et al., 2005) and higher HOM yields (Wang et al., 2017;Molteni

338   et al., 2018) than their homologues with less carbon atoms. In terms of molecular

339   formula, the aromatics-derived OOMs have an overlap with monoterpenes-derived

340   OOMs (Mehra et al., 2020). Monoterpenes can contribute more C_{10} OOMs than

341   aromatics ($P_{MT-RO_2} > P_{C_{10}\ Aro-RO_2}$), but aromatics play a more important role in total

342   in this factor since they provide more RO_2 in the urban atmosphere (Fig. 3(f)).

343

344 $$P_{RO_2} = k_{OH+VOC} \bullet [OH] \bullet [VOC] \tag{4}$$

345

346
347   Figure 3. Mass spectra of (a) the Aro-OOMs factor, (b) the Temp-related factor, (c) the
348   Aliph-OOMs factor, and the elemental formulas of major peaks are labeled above them.
349   Peaks are color-coded by n_N as indicated at the top right of the figure, and the fractions
350   of peaks grouped by n_N are reported in (d) the pie chart. The gray sticks are fluorinated
351   contaminations, or non-identified compounds. The nitrated phenols are drawn
352   separately with black peaks in (a), (b) and (c), and were not included in (d). So nN can
353   more reliably represent the number of nitrate groups in each molecule. Diurnal patterns
354   (Beijing time) of these three factors are shown in (e), the bold solid lines are the median
355   values, shaded areas represent percentiles of 75 % and 25 % and solid circles represent
356   mean values.

357

358   The main molecules of the Aro-OOMs factor are summarized in Table S2. The $C_xH_{2x-5}O_6N$

359   (x=6-12, of which $C_8H_{11}O_6N$ is the most intense) series can be produced by the

360   reaction (R1a) of NO with the bicyclic peroxy radicals (HO-Ar-$(O_2)_2$), the key

361   intermediates for aromatics oxidation proposed in the MCM (Bloss et al., 2005;Birdsall

362   and Elrod, 2011). And here dihydroxy nitro-BTEX ($C_xH_{2x-7}O_4N$, x=6-8) can be treated

363 as indicators of aromatics oxidation. In addition to the conventional products, $C_9H_{13}O_{7-9}N$
364 from the $C_xH_{2x-5}O_{7-9}N$ (x=7-13) series are also significant in the OH-initiated and
365 NO$_x$-influenced oxidation experiments of 1,2,4-trimethylbenzene (Zaytsev et al.,
366 2019) and of 1,3,5-trimethylbenzene (Tsiligiannis et al., 2019). More oxygenated
367 compounds may come from auto-oxidation and multigenerational OH attacks. However,
368 the effective OSc of this factor (Table 1) is lower than that of oxidation products of
369 aromatics in recent laboratories (Zaytsev et al., 2019;Tsiligiannis et al., 2019;Garmash
370 et al., 2020;Wang et al., 2020c). We speculate that the abundances of NO$_x$ relative to
371 oxidants and precursors in these experiments are not sufficient to reproduce the
372 atmospheric conditions during our observation, or that HOMs are more concentrated in
373 aerosols due to the large condensation sink on this site (Qi et al., 2015). Although
374 species with DBE < 3 (Fig. 2(b)) in this factor are most likely produced from multiple
375 OH attacks in aromatics oxidation, we can't rule out the contribution of alkanes co-
376 emitted with aromatics, such as the series $C_xH_{2x-1}O_6N$ (x=5-14).

377
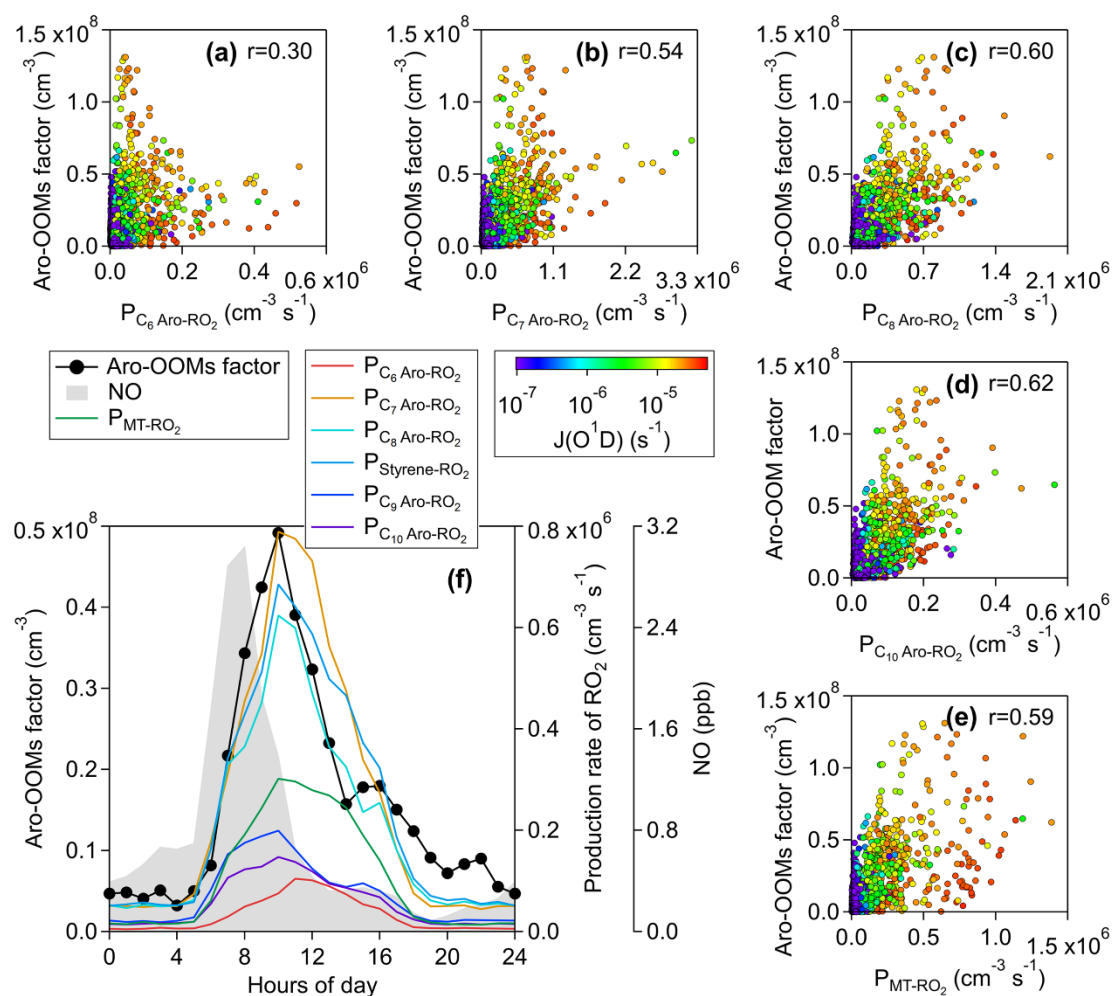
378
379 Figure 4. Correlations of the Aro-OOMs dominated factor with production rate of RO$_2$
380 from OH-initiated oxidation of (a) benzene ($P_{C_6\ Aro-RO_2}$), (b) toluene ($P_{C_7\ Aro-RO_2}$), (c)
381 C_8 aromatics ($P_{C_8\ Aro-RO_2}$), (d) C_{10} aromatics ($P_{C_{10}\ Aro-RO_2}$), and (e) Monoterpenes

(P_{MT-RO_2}). All the scatters are colored by $J(O^1D)$, to show the difference between day and night. The median diurnal patterns of this factor and related parameters are plotted in (f).
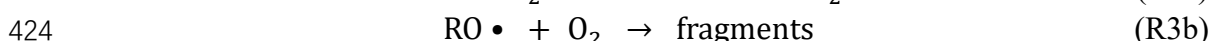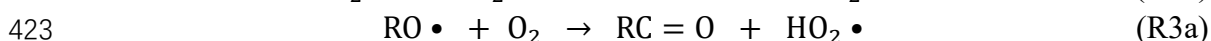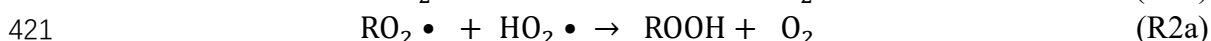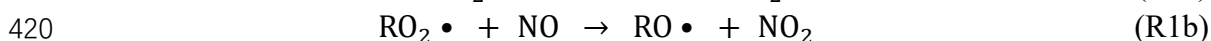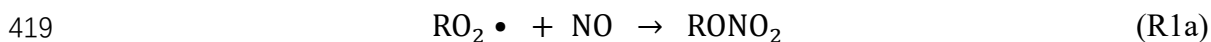
Temp-related factor

This factor is named due to good correlation with temperature (Fig. 5), and shows maximum intensity in the afternoon around 15:00 (Fig. 3(e)). The Temp-related factor is the only one dominated by non-nitrogenous organics (Fig. 3(b) and (d)), and has the highest effective OSc (Table 1) among all the factors. The $C_xH_{2x-4}O_5$ (x=5-11, summarized in Table S3), $C_xH_{2x-2}O_5$ (x=5-10), $C_xH_{2x-6}O_5$ (x=5-11), and $C_xH_{2x-4}O_6$ (x=5-10) series are possibly products from RO_2 terminated by HO_2 (R2a), or closed-shell products from RO in reactions R3a or R3b. Temperature starts to rise at 6:00 LT (Fig. 12(b)), but this factor does not accumulate significantly until after about 10:00 LT (Fig. 3(e)), when the mixed level of NO is reduced to 1 ppb (Fig. 4(f)). This phenomenon suggests a probability of HO_2-driven chemistry of this factor under low NO conditions, since that NO can consume HO_2 and compete with HO_2 for RO_2. Such low-NO atmospheric oxidation pathways have been suggested to be non-negligible in the afternoon in central Beijing (Newland et al., 2021).
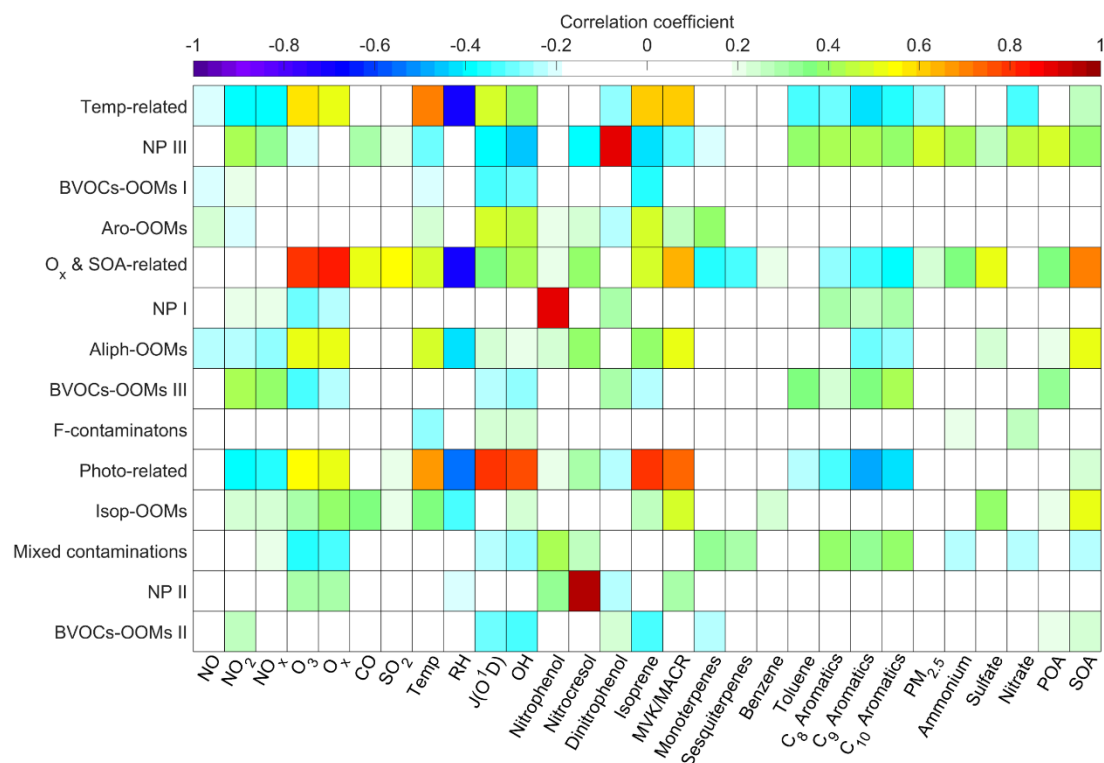
A factor caused by similar chemical processes called isoprene afternoon was discovered in the nitrate CI-APi-TOF data collected at a forest site in Centreville, Alabama, USA (Massoli et al., 2018), correlated well with HO_2, O_3, and temperature. We also observed a number of isoprene oxidation products in the Temp-related factor (nC = 4, 5 in Fig. 2(a)). Many of the $C_xH_{2x-1}O_6N$ (x=3-7) and $C_xH_{2x-3}O_6N$ (x=4-9) series were also present in the light HOMs factor which was supposed to be fragments from the oxidation of larger VOCs (e.g., monoterpene) in Hyytiälä, Finland (Yan et al., 2016). While at the SORPES station, the C_6-C_9 ions should mainly come from the oxidation of anthropogenic VOCs. At lower temperatures, the propensity of condensable organic molecules to condense into aerosol makes the concentration measured using nitrate CI-APi-TOF lower. Thus, the total concentration of the Temp-related factor in the gas and aerosol phases was calculated based on gas-particle equilibrium (section S5 in the supplement), and was found to be still temperature dependent (Fig. S7), illustrating the temperature-influenced chemical process controlling the factor. For instance, Unimolecular reaction rates like RO_2 H-shifts increase qualitatively with temperature (Bianchi et al., 2019;Frege et al., 2018).

$$RO_2\bullet \ + \ NO \ \rightarrow \ RONO_2 \qquad\qquad (R1a)$$
$$RO_2\bullet \ + \ NO \ \rightarrow \ RO\bullet \ + \ NO_2 \qquad\qquad (R1b)$$
$$RO_2\bullet \ + \ HO_2\bullet \ \rightarrow \ ROOH + \ O_2 \qquad\qquad (R2a)$$
$$RO_2\bullet \ + \ HO_2\bullet \ \rightarrow \ RO\bullet \ + \bullet OH + \ O_2 \qquad\qquad (R2b)$$
$$RO\bullet \ + \ O_2 \ \rightarrow \ RC=O \ + \ HO_2\bullet \qquad\qquad (R3a)$$
$$RO\bullet \ + \ O_2 \ \rightarrow \ fragments \qquad\qquad (R3b)$$

426

Figure 5. Correlations of PMF factors with external gas-phase and particulate tracers
from other instruments deployed at the SOPRES station, with the color representing the
Pearson correlation coefficients. From left to right, the tracers are gas-phase species
(NO, NO_2, NO_x, O_3, CO, SO_2), meteorological data (temperature (Temp), relative
humidity (RH), photolysis constants ($J(O^1D)$)), nitrate CI-APi-TOF data (OH,
nitrophenol, nitrocresol, dinitrophenol), PTR-ToF-MS data (isoprene, methyl vinyl
ketone/methacrolein (MVK/MACR)), monoterpenes, sesquiterpenes, benzene, toluene,
C_8 aromatics, C_9 aromatics, C_{10} aromatics), $PM_{2.5}$, and ACSM data (ammonium, sulfate,
nitrate, POA, SOA).

Aliph-OOMs factor

This factor is dominated by organic nitrates (Fig. 3(c) and (d)), and contains the bulk
of anthropogenic di-nitrates and tri-nitrates. The $C_xH_{2x-2}O_8N_2$ (x=4-13, summarized in
Table S4) and $C_xH_{2x}O_8N_2$ (x=4-9) series have not been reported in aromatics oxidation
experiments under high NO_x conditions (Tsiligiannis et al., 2019;Wang et al., 2020c),
and nor in the forest or rural environments (Yan et al., 2016;Massoli et al., 2018). A
reasonable assumption is that these saturated or nearly saturated compounds are the
products of aliphatics (including alkanes, alkenes, aliphatic alcohol, etc.) during their
oxidation affected intensively by NO_x in the urban atmosphere. The Aliph-OOMs factor
has a broad afternoon peak lasting from 14:00 to 19:00 LT (Fig. 3(e)), suggesting that
the formation of multi-nitrate requires enough OH exposure time.

Considering a simple scenario of alkane photo-oxidation under high NO_x conditions:

the RO_2 generated from OH attack is completely terminated by NO (Fig. 6(a)). The
chain-retaining products are $C_nH_{2n}O$ (one more carbonyl group than the precursor) and
$C_nH_{2n+1}O_3N$ (one more nitrate group than the precursor), and the re-oxidation of these
products is a repetition of the above process which is defined as the basic reaction
scheme. The multiple (1st to 3rd) generation products of alkanes summarized in Fig.
6(b) are regarded as reference compounds, which we compare OOMs with to
investigate other mechanisms that differ from those shown in Fig. 6(a). Specifically,
this comparison is performed between the reference molecule and OOMs with the same
numbers of carbon, hydrogen and nitrogen atoms, but different numbers of oxygen

atoms. The number of extra oxygen ($n_{O_{extra}}$) from each aliphatic OOM over its

corresponding reference molecule was calculated by Eq. (5), that is, subtracting

carbonyl and nitrate oxygens from the molecule. Thus, the $n_{O_{extra}}$ can represent the

additional oxygenated moieties such as hydroxyl group (-OH), peroxy group (-OOH),
and possibly ether group. These functional groups may come from RO isomerization
(Orlando et al., 2003), the addition of OH to alkenes, or pre-existing moieties in the
precursor, RO_2 autoxidation or specific RO_2 bimolecular termination reactions
(RO_2+RO_2, RO_2+HO_2).

$$n_{O_{extra}} = n_O - DBE - 3 \times n_N \qquad (5)$$

As showed in Fig. 6(c), aliphatic OOMs in this factor are mainly the third-generation
products followed by the second-generation products, and both of which have one or
two oxygen-containing functional groups in addition to the carbonyls and nitrates. It
should be noted that the first-generation (Fig. 6(a)) and basic products (Fig. 6(b)) here
are underestimated due to the low sensitivity of nitrate CI-APi-TOF to these compounds.
The multifunctional products of aliphatics are condensable to form SOA (correlation
coefficients with SOA showed in Fig. 5). Recent work has showed that autoxidation is
more common than previously thought (Wang et al., 2021), and more studies are needed
to explore the oxidation mechanisms of anthropogenic aliphatics and to evaluate their
contribution to SOA.
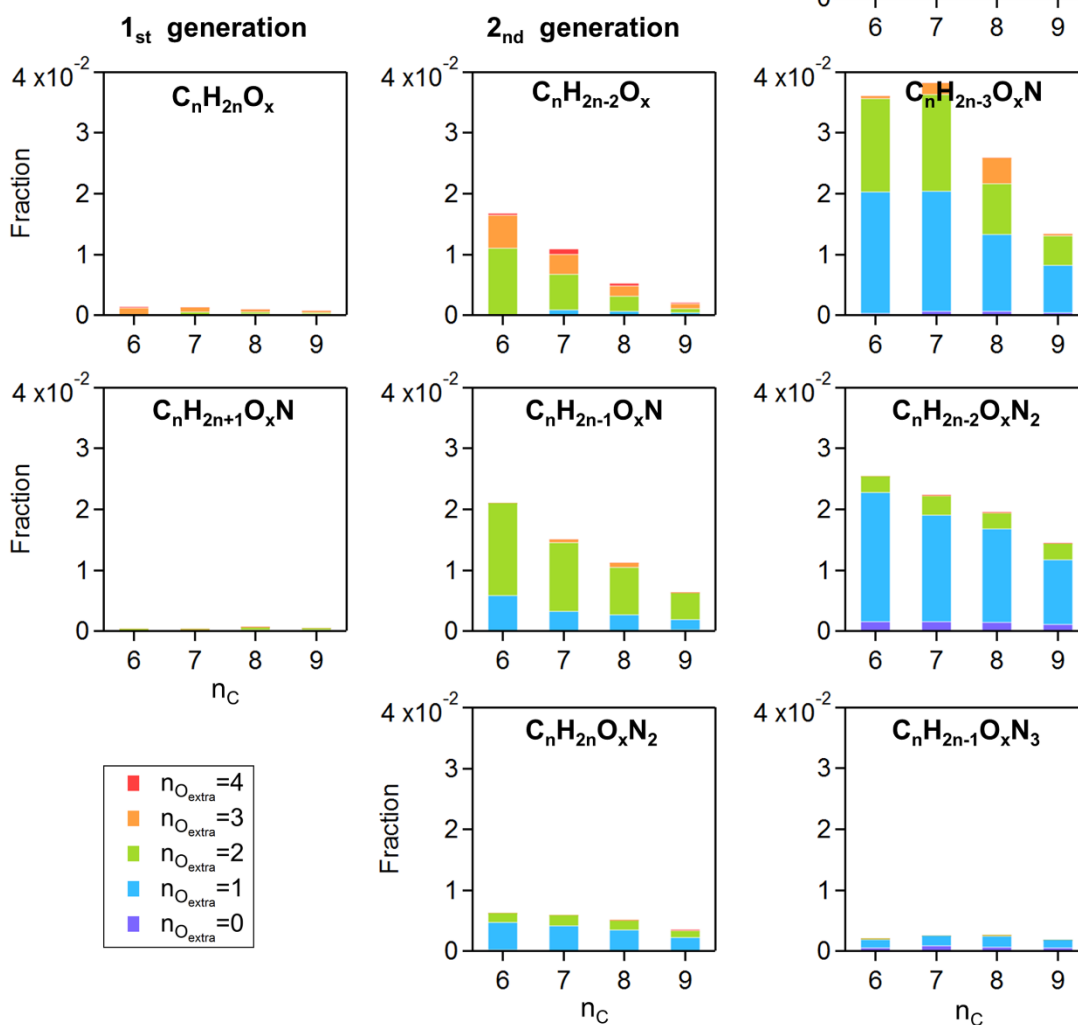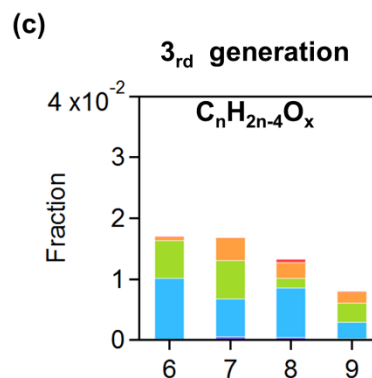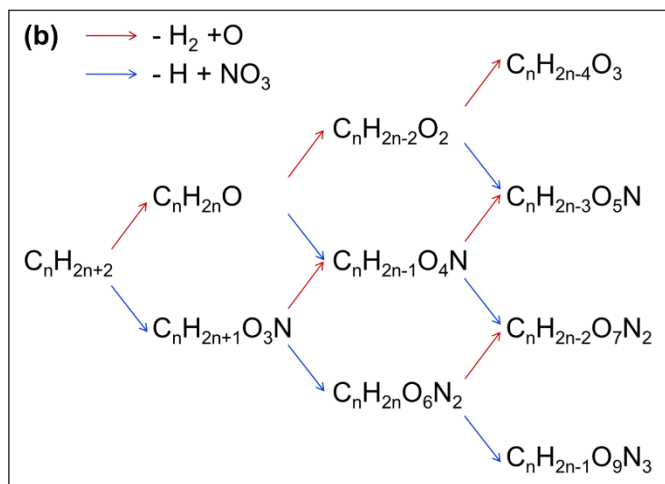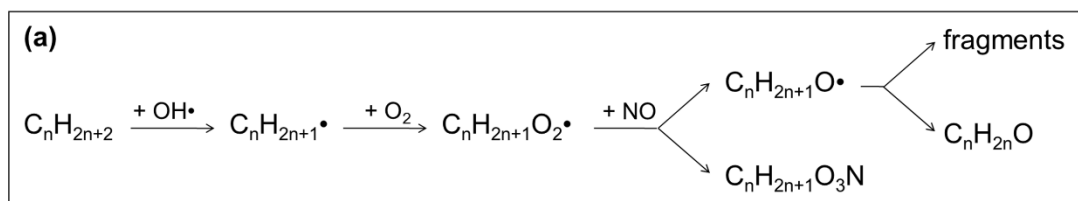
484   Figure 6. (a) Simplified oxidation mechanism for alkanes attacked by OH once under

485 NO_x-controlled conditions. (b) summarizes the changes in molecular formula of the 1st
486 to 3rd generation products of alkanes, based on the basic reaction scheme in (a). (c)
487 shows the fraction of potential alkanes-derived compounds in the Aliph-OOMs factor.
488 The compounds listed in (c) are grouped according to the molecular formulas in (b),
489 i.e., the same number of carbon, hydrogen and nitrogen atoms, but different numbers

490 of oxygen atoms. The bars in (c) are colored with $n_{O_{extra}}$. Please see text for details

491 about $n_{O_{extra}}$.

492
493 **3.2 Isoprene-related chemistry**

494
495 The following factors are characterized by C_5 OOMs (Fig. 2(a)), of which an isoprene
496 dihydroxyl dinitrate $C_5H_{10}O_8N_2$ (charged by NO_3^- at m/z 288 Th) is the fingerprint
497 molecule (Fig. 7). Apart from isoprene-derived compounds, OOMs formed from other
498 precursors undergoing the similar chemical processes are also allocated to these three
499 factors.

500
501 **Photo-related factor**

502
503 This factor is defined based on its correlation with $J(O^1D)$ (Fig. 5), having an apparent
504 diurnal cycle with a peak at 12:00 LT (Fig. 7(e)). The major peak of the Photo-related
505 factor is $C_5H_{10}O_8N_2$ (Fig. 7(a)), most probably generating from double OH attack
506 proceed with double RO_2+NO termination (Jenkin et al., 2015). $C_5H_{10}O_8N_2$ can be also
507 produced in NO_3+ isoprene system (Ng et al., 2008;Zhao et al., 2020), whereas in this
508 study, the nocturnal $C_5H_{10}O_8N_2$ is principally from the Isop-OOMs factor (Fig. 8(b))
509 which will be discussed later. Other peaks with nC≤5, like $C_5H_7O_7N$, $C_4H_7O_6N$,
510 $C_5H_9O_6N$, are also likely to be the isoprene products. The total signal of compounds
511 with nC > 5 is not low, although their respective proportions are not as prominent as C_5
512 species (Fig. 7(d)), implying the contribution of other precursors together with isoprene.
513 In addition, the relationship of this factor with isoprene and $J(O^1D)$ together (Fig. 5)
514 reveals the effect of light-dependent emission of isoprene on it.

515
516 **O_x & SOA-related factor**

517
518 The atmospheric oxidation of VOCs produces low-volatile compounds, forming SOA
519 through gas-particle partitioning, and concurrently promotes ozone formation
520 (Atkinson, 2000). Both SOA and O_x have long lifetimes (>12 h), and their correlations
521 have been extensively investigated (Herndon et al., 2008;Wood et al., 2010;Hu et al.,
522 2016). The OOMs factor related to ozone and SOA together (Fig. 5), having slightly
523 elevated concentrations during daytime (Fig. 7(e)), is considered to be generated from
524 this photochemical aging process. Apart from $C_5H_{10}O_8N_2$, other isoprene multi-nitrates
525 are also present in this factor. $C_5H_9O_{10}N_3$, an isoprene hydroxyl trinitrate requiring at
526 least two steps of oxidation found in the experimental study on isoprene oxidation by

NO3 (Zhao et al., 2020), naturally does not appear in the photo-related factor at all, but is mostly apportioned into the O_x & SOA-related factor and the Isop-OOMs factor (Fig. 8(c) and 8(d)). Like the photo-related factor, isoprene is a significant but not the only precursor of this factor (Fig. 2 and 7). The biggest peak of the O_x & SOA-related factor is an ion at m/z 264 with formula $C_6H_5O_3N$ ($HNO_3NO_3^-$), identified as an adduct of nitrophenol ($C_6H_5O_3N$) with nitrate dimmer ($HNO_3NO_3^-$). The time variation of $C_6H_5O_3N$ ($HNO_3NO_3^-$) is influenced by the reagent ions in addition to the atmospheric nitrophenol. So far, we don't know why this compound share the same processes with others, but we did a test that removing the bins with unit m/z = 264 from the input matrix and still got this factor from PMF model.
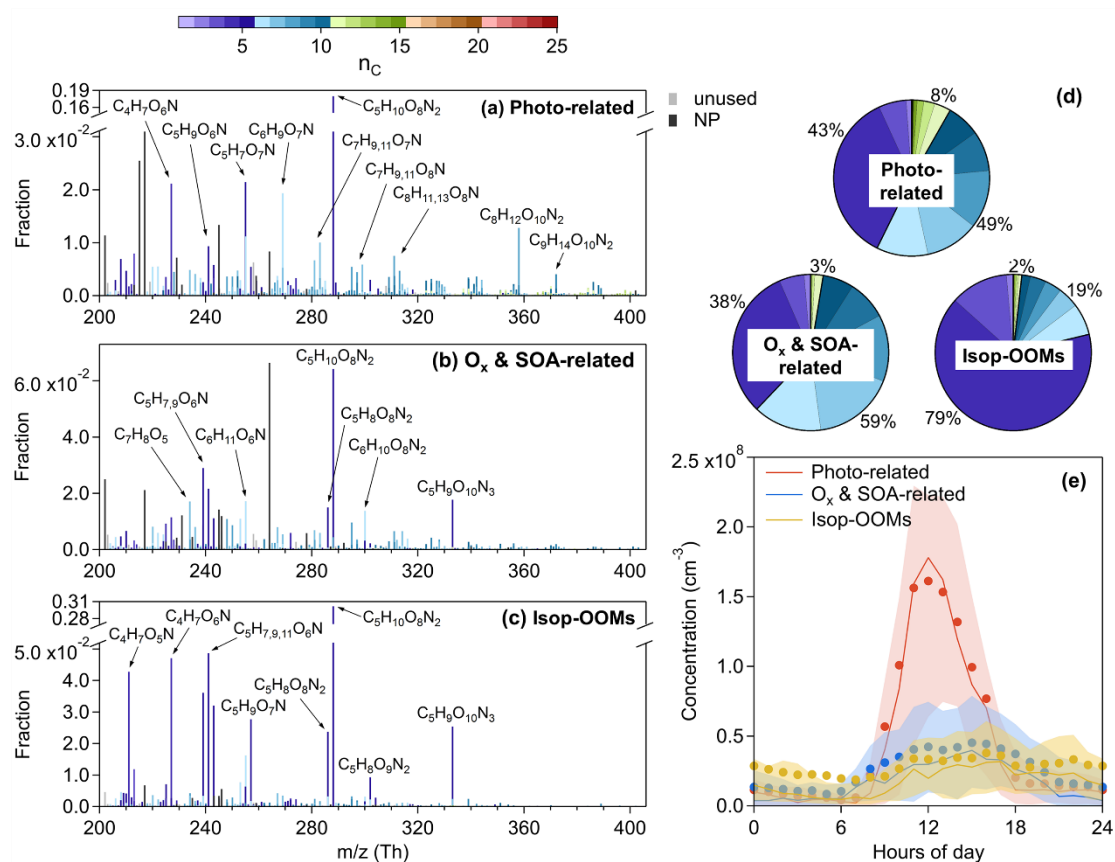
Figure 7. Mass spectra of (a) the Photo-related factor, (b) the O_x & SOA-related factor, (c) the Isop-OOMs factor, and the elemental formulas of major peaks are labeled above them. Peaks are color-coded by n_C as indicated at the top of the figure, and the fractions of peaks grouped by n_C are reported in (d) the pie chart. The gray sticks are fluorinated contaminations, or non-identified compounds. The nitrated phenols are drawn separately with black peaks in (a), (b) and (c). The molecules represented by the gray and black sticks were not included in (d). Diurnal patterns of the three factors are shown in (e), the bold solid lines are the median values, shaded areas represent percentiles of 75 % and 25 % and solid circles represent mean values.

Isop-OOMs factor

551 The mass spectra of the Isop-OOMs factor, as its name implies, is exclusively
552 contributed by isoprene-derived compounds (Fig. 7(c)). $C_5H_{10}N_2O_8$ contributes about
553 30% of the intensity of this factor, and the dominance of $C_5H_{10}N_2O_8$ was also found in
554 the isoprene nitrates type I factor in Centreville (Massoli et al., 2018). In addition to
555 multi-nitrates ($C_5H_{10}O_{7-8}N_2$, $C_5H_8O_{6-9}N_2$, and $C_5H_9O_{10}N_3$ summarized in Table. S6),
556 several mononitrate series ($C_4H_7O_{5-7}N$, $C_5H_9O_{4-9}N$, $C_5H_7O_{5-8}N$, and $C_5H_{11}O_{5-6}N$) of
557 this factor are also abundant in the isoprene nitrates type II factor in Centreville
558 (Massoli et al., 2018). Many of isoprene nitrates here have been specially investigated
559 in our previous observations in the YRD (Xu et al., 2021), and have been discovered in
560 other filed measurements (Lee et al., 2016;Massoli et al., 2018) and in many
561 laboratories (Ng et al., 2008;Lambe et al., 2017). Generally, these compounds are
562 second- and third-generation OH oxidation products of isoprene under high-NO_x
563 conditions (Wennberg et al., 2018).
564
565 The diurnal pattern of the Isop-OOMs factor is relatively unclear (Fig. 7(e)), with
566 obvious differences between mean and median values usually caused by plume events.
567 This indicates that isoprene chemistry, usually varying evidently from day (OH-
568 initiated) to night (NO_3-initiated), is not the driver of this factor. This factor correlates
569 positively with MVK / MACR and SOA (r>0.50, showed in Fig. 5), but not with
570 isoprene and OH. It seems that these isoprene OOMs are produced elsewhere and then
571 transported due to their longer lifetime determined by their relatively high volatility
572 (Table 1). The Isop-OOMs factor in the continental air masses are more intensive than
573 those in the coastal and YRD air masses (Fig. S8), consistent with the spatial
574 distribution of isoprene emissions (Sindelarova et al., 2014). An archetypal episode
575 affected by continental air masses (August 13 to August 17, 2019) is showed in Fig. 8.
576 During this period, $C_5H_9O_{10}N_3$ was almost entirely transported, while $C_5H_{10}O_8N_2$ has
577 strong in situ photochemical generation, in addition to the source of transport.
578
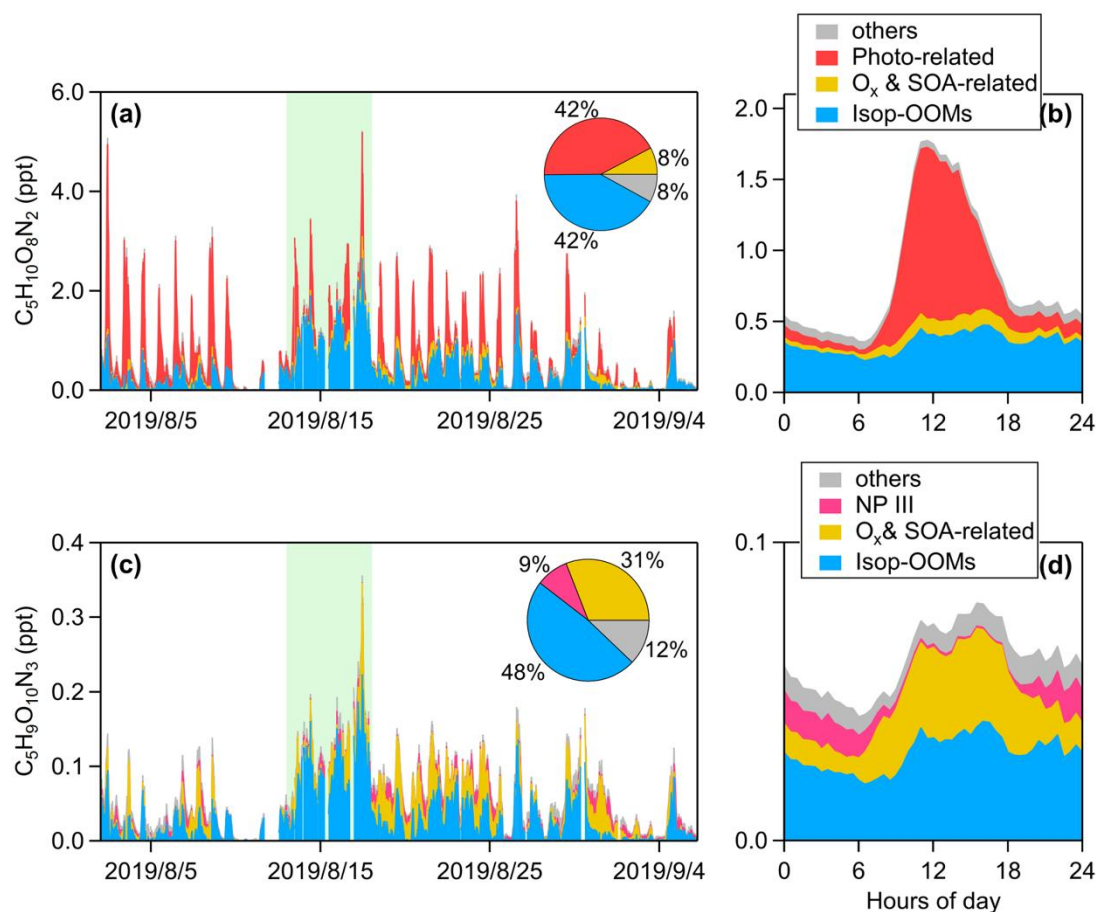
Figure 8. Stacked (a) time series and (b) mean diurnal pattern of isoprene dihydroxyl dinitrate ($C_5H_{10}O_8N_2$). Stacked (c) time series and (d) mean diurnal pattern of isoprene hydroxyl trinitrate ($C_5H_9O_{10}N_3$). The contribution ratios of each PMF factor to these two compounds are reported in the pie chart respectively. The light green shaded area represents a typical episode influenced by transported continental air masses (August 13 to August 17, 2019).

3.3 BVOCs nighttime chemistry

The following nighttime factors are characterized by C_{10} OOMs (Fig. 2(a)), which are identified as the oxidation products of monoterpenes. Except for the BVOCs-OOMs I factor (Fig. 9(a)), the contribution of isoprene-derived OOMs was much lower in these factors. Compared to the above isoprene-related factors, $C_5H_{10}O_8N_2$ and $C_5H_9O_{10}N_3$ was no longer significantly present in the following factors.

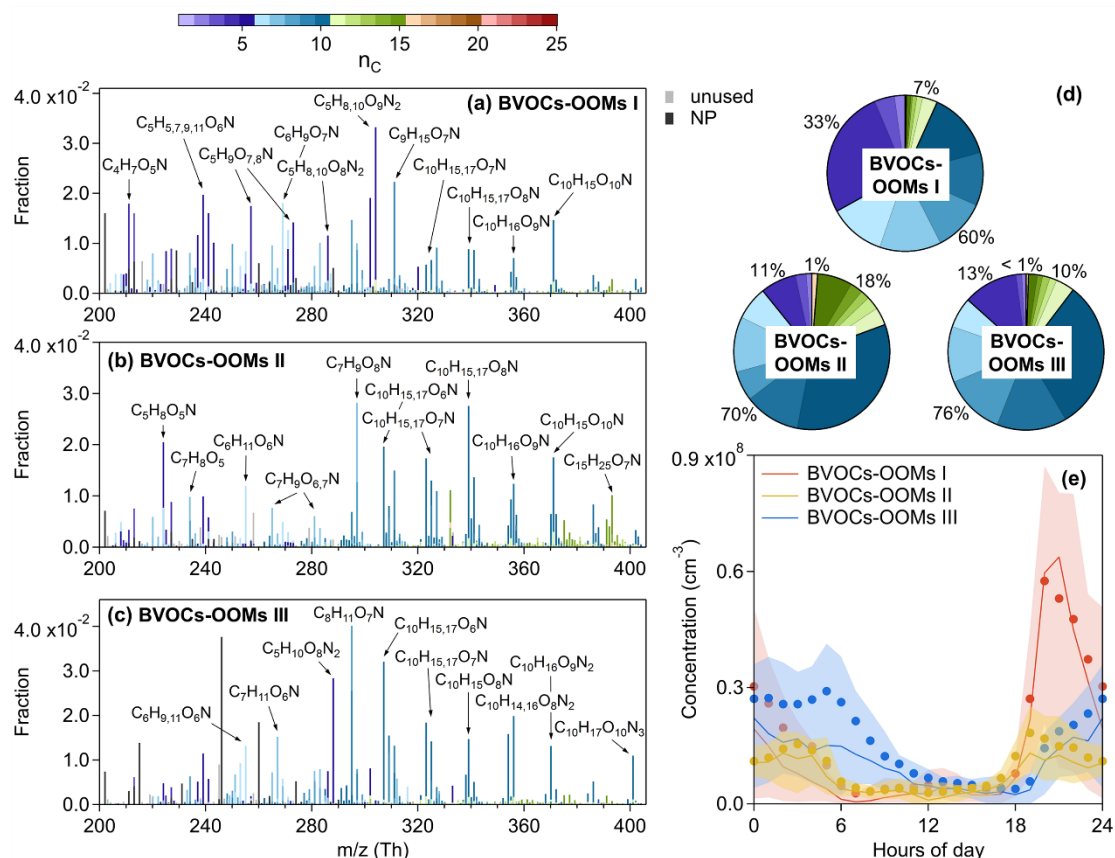**BVOCs-OOMs I factor**

The first nighttime factor has its maximum concentration at around 20:00 LT, and decreases to very low value during the day. It is moderately correlated with the production rate of NO_3 radical (P_{NO_3} derived from Eq. 6) at night, and reaches high intensity only under conditions of NO below 1 ppb (Fig. 10(a)), indicating a chemical

process of NO$_3$ radical. The concentration of this factor is mainly from C$_5$ peaks, followed by C$_6$-C$_{10}$ peaks (Fig. 9(d)), about 80% of which are ONs (Fig. 2(c)), designating the oxidations of isoprene and monoterpenes by NO$_3$ (BVOCs-OOMs I). In the case of isoprene oxidation, the nitrate groups of C$_5$H$_9$O$_{4-8}$N, C$_5$H$_7$O$_{5-8}$N and C$_4$H$_7$O$_{5-6}$N series (summarized in Table S8) are likely to come from the addition of NO$_3$. Next, the C$_5$H$_{10}$O$_{8-9}$N$_2$ and C$_5$H$_8$O$_{7-10}$N$_2$ series are probably second-generation products. These compounds derived from isoprene+NO$_3$ system have been discussed in previous laboratory (Kwan et al., 2012;Zhao et al., 2020) and ambient data sets (Ayres et al., 2015;Xiong et al., 2015). Additionally, The C$_6$-C$_{10}$ species are potentially the products of monoterpenes degraded by NO$_3$.

$$P_{NO_3} = \ k_{NO_2+O_3} \bullet [NO_2] \bullet [O_3] \tag{6}$$

Figure 9. Mass spectra of (a) the BVOCs-OOMs I factor, (b) the BVOCs-OOMs II factor, (c) the BVOCs-OOMs III factor, and the elemental formulas of major peaks are labeled above them. Peaks are color-coded by n$_C$ as indicated at the top of the figure, and the fractions of peaks grouped by n$_C$ are reported in (d) the pie chart. The gray sticks are fluorinated contaminations, or non-identified compounds. The nitrated phenols are drawn separately with black peaks in (a), (b) and (c). The molecules represented by the gray and black sticks were not included in (d). Diurnal patterns of these three factors are shown in (e), the bold solid lines are the median values, shaded areas represent percentiles of 75 % and 25 % and solid circles represent mean values.
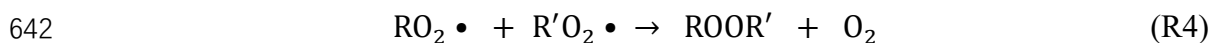
BVOCs-OOMs II factor
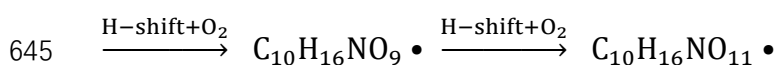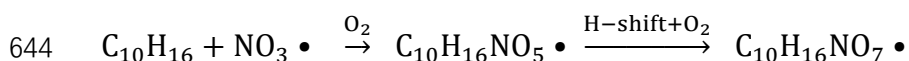
The second nighttime factor are intense at night and over five times lower during the day. Like the BVOCs-OOMs I factor, this factor has high concentrations when NO is reduced leading to increased NO_3 availability (Fig. 10(b)), and about 80% of compounds in this factor are ONs (Fig. 2 (c)). Accordingly, this may also be a factor strongly influenced by NO_3. It is dominated by C_6-C_{10} OOMs, among which the highest intensity is at C_{10} (Fig. 9(d)), coherent with the nature of monoterpene products (BVOCs-OOMs II). This factor has weaker signals at C_{15} which are plausibly the products of sesquiterpenes but could also be dimmers formed from R4 (monoterpenes + isoprene or monoterpenes + C_5 monoterpenes fragments). Compared to the BVOCs OOMs I factor (Fig. 9(d)), this factor has more large mass molecules (C_{10}) and fewer small mass molecules (C_5), resulting in an effective volatility over one order of magnitude lower.   A NO_3-initiated factor, called the nighttime type-2 factor, has also been discovered in Hyytiälä, Finland (Yan et al., 2016), but the similar factor we found has a higher proportion of organic nitrates, due to the more abundant NO_x here.
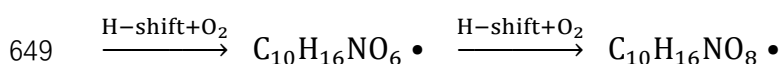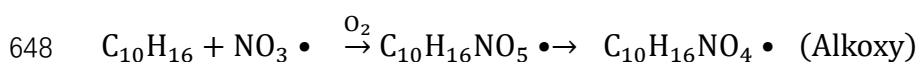
$$RO_2 \bullet \ + \ R'O_2 \bullet \ \rightarrow \ ROOR' \ + \ O_2 \qquad\qquad (R4)$$

$$C_{10}H_{16} + NO_3 \bullet \ \xrightarrow{O_2} \ C_{10}H_{16}NO_5 \bullet \ \xrightarrow{H-shift+O_2} \ C_{10}H_{16}NO_7 \bullet$$

$$\xrightarrow{H-shift+O_2} \ C_{10}H_{16}NO_9 \bullet \ \xrightarrow{H-shift+O_2} \ C_{10}H_{16}NO_{11} \bullet$$

(R5a)

$$C_{10}H_{16} + NO_3 \bullet \ \xrightarrow{O_2} C_{10}H_{16}NO_5 \bullet \rightarrow \ C_{10}H_{16}NO_4 \bullet \ \ (Alkoxy)$$

$$\xrightarrow{H-shift+O_2} \ C_{10}H_{16}NO_6 \bullet \ \xrightarrow{H-shift+O_2} \ C_{10}H_{16}NO_8 \bullet$$

(R5b)

In terms of fingerprint molecules of this factor (summarized in Table S9), The $C_{10}H_{15}O_{5-12}N$ series are carbonyl products from precursor RO_2 or RO terminations, while the $C_{10}H_{17}O_{5-9}N$ series are alcohol or hydroperoxide products from precursor RO_2 terminations. The $C_7H_9O_{6-8}N$, $C_9H_{15}O_{6-9}N$, $C_9H_{13}O_{7-10}N$, and $C_8H_{13}O_{7-8}N$ series are expected to be fragments. The closed-shell compounds mentioned above have been reported in the experiments of monoterpenes + NO_3 system (Nah et al., 2016;Faxon et al., 2018;Takeuchi and Ng, 2019).

It is noteworthy that a set of nitrogen-containing radicals, $C_{10}H_{16}O_{6-11}N$ (peak fitting are shown in Fig. S9), is present in the BVOCs-OOMs II factor. Starting from a generic monoterpene molecule with the formula $C_{10}H_{16}$, the NO_3 addition with fast O_2 addition results in a peroxy radical with the formula $C_{10}H_{16}O_5N$, If the initial intermediate RO_2

664 is capable to proceed via autoxidation by the formal addition of O_2, we expect radicals,
665 $C_{10}H_{16}O_{5+2x}N$ (x denotes times of autoxidation performed) with an odd oxygen number,
666 to be formed (R5a). In addition, peroxy radicals with an even oxygen number,
667 $C_{10}H_{16}O_{6+2x}N$, are likely produced via reaction chain 5b: (1) RO_2 is propagated to RO
668 through bimolecular reactions, and (2) RO isomerize to an alcohol by internal H
669 abstraction forming a carbon-centered radical (Orlando et al., 2003;Orlando and
670 Tyndall, 2012), (3) the carbon-centered radical can again take up an oxygen molecule
671 and follow the autoxidation route. The $C_{10}H_{16}O_9N$ radical is also moderately intense in
672 the BVOCs-OOMs I factor (Fig. 9(a)), testifying the presence of NO_3 chemistry. These
673 $C_{10}H_{16}O_{6-11}N$ radicals are also reported in the CLOUD chamber (Yan et al., 2020). In
674 addition to C_{10} radicals, a C_5 radical, $C_5H_8O_5N$ (peak fitting are shown in Fig. S9), is
675 also found in the BVOCs-OOMs II factor. $C_5H_8O_5N$ are possibly derived from the
676 oxidation of isoprene initiated by NO_3, as observed in the laboratory (Zhao et al., 2020).
677 Another hypothesis is that $C_5H_8O_5N$ is formed from the fragmentation process of
678 monoterpenes.
679
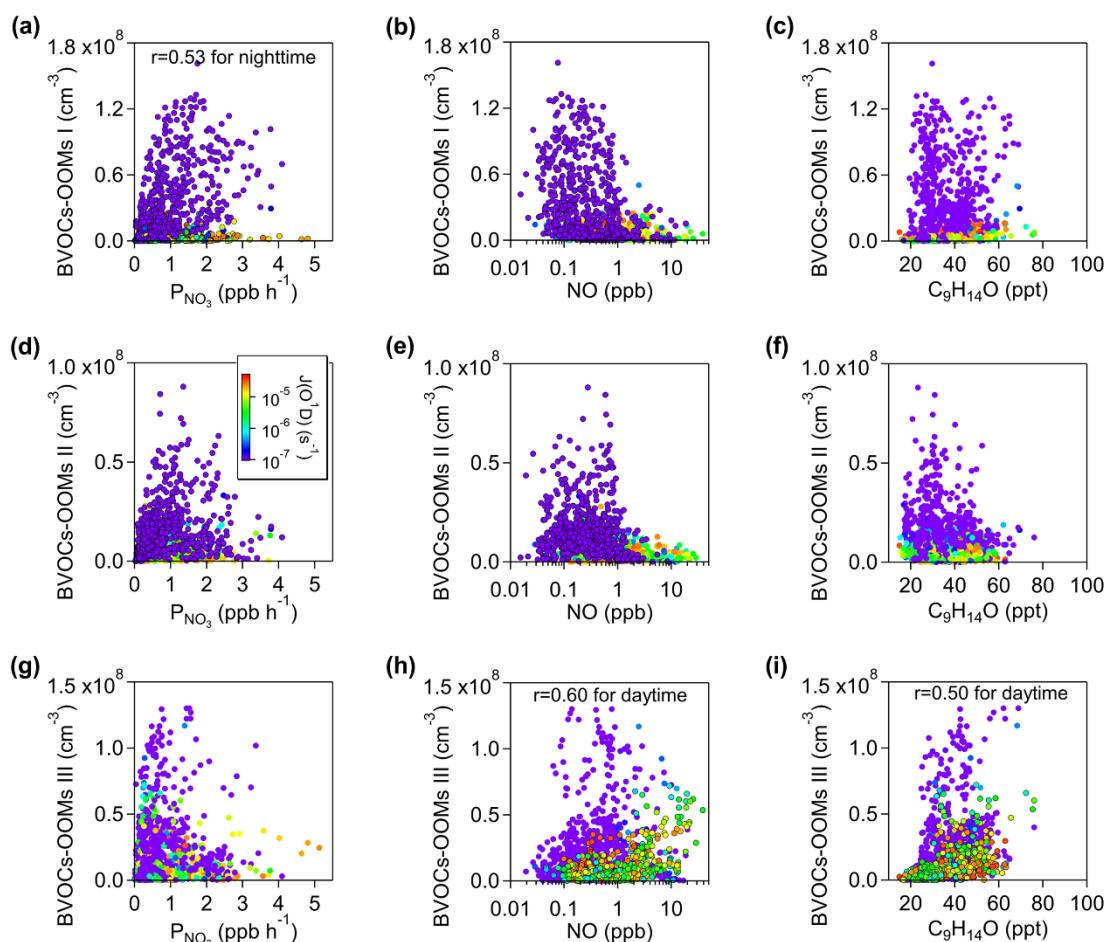
680

681 Figure 10. Scatter plots of the BVOCs-OOMs I factor with (a) P_{NO_3}, (b) NO, and (c)

682 nopinone ($C_9H_{14}O$). Scatter plots of the BVOCs-OOMs II factor with (d) P_{NO_3}, (e) NO,

683 and (f) nopinone ($C_9H_{14}O$). Scatter plots of the BVOCs-OOMs III factor with (g) P_{NO_3},

684 (h) NO, and (i) nopinone ($C_9H_{14}O$). All the scatters are colored by $J(O^1D)$, to show the
685 difference between day and night. Pearson correlation coefficient showed in (a) is
686 calculated for nighttime, but the correlation coefficients in (c) are only for daytime.

BVOCs-OOMs III factor

690 The third nighttime factor (BVOCs-OOMs III) is dominated by nitrogen-containing
691 species with a contribution ratio about 90%, among which dinitrates account for more
692 than 20% (Fig. 2(c)). When grouped by carbon numbers, C_{10} OOMs have the strongest
693 signal. Unlike the above two NO_3-related factors, this factor shows no correlation with
694 P_{NO3}, but has positive correlation with NO, especially during the daytime (Fig. 10(c)).
695 $C_9H_{14}O$, a typical product of NO-affected monoterpenes oxidation (Calogirou et al.,
696 1999), is found to be correlated with this factor (Fig. 10(c)). It is reasonable to infer that
697 these organic nitrates may come from terminations of monoterpenes-RO_2 by NO. In
698 addition to the elevated intensity during the nighttime, this factor still remains at a
699 relatively high concentration in the morning, which is much higher than that of the two
700 NO_3-related factors (Figure 9(e)). Owing to the suppression of NO to RO_2 autoxidation
701 and the relatively insufficient oxidant in dark environment, the effective OSc of the
702 BVOCs-OOMs III factor is lower than other factors. Apart from the mononitrates
703 summarized in Tabel S10, the $C_{10}H_{16}O_{7-10}N_2$ (dinitrates) and $C_{10}H_{17}O_{10}N_3$ (a trinitrate
704 charged by NO_3^- at m/z 401) are most likely the result of multiple-generation processes
705 involving OH or NO_3 oxidation of monoterpenes proceeding RO_2 + NO terminations.
706 A similar factor, called terpene nitrates, has also been reported in Centreville, USA
707 (Massoli et al., 2018), while in Hyytiälä, Finland (Yan et al., 2016), it's that the daytime
708 type-1 factor is related to NO.

3.4 Nitrated phenols factors

712 Nitrated phenols are of concern, because of their phytotoxicity (Rippen et al., 1987)
713 and as an important chromophores of brown carbon in aerosol (Desyaterik et al.,
714 2013;Mohr et al., 2013). The sources of these highly volatile compounds are attributed
715 to biomass burning, vehicle exhausts, and secondary gas or aqueous phase production
716 (Harrison et al., 2005). Here we identified three factors about NP, including the NP I
717 factor dominated by nitrophenol, the NP II factor dominated by substituted nitrophenols,
718 and the NP III factor dominated by dinitrophenols. Although the mass spectrum of the
719 NP III factor is less pure than the NP I & II factors (Fig. 11), its time series follows well
720 with $C_6H_4O_5N_2$ (Fig. 11(f)), implying that this factor is driven by di-nitrated-phenols
721 chemistry. Since nitrated phenols have been broadly investigated and relatively clearly
722 recognized (Harrison et al., 2005;Yuan et al., 2016;Wang et al., 2018b;Cheng et al.,
723 2021), they are not discussed too much here. It seems that the chemistry of nitrated
724 phenols is distinctive to other OOMs.
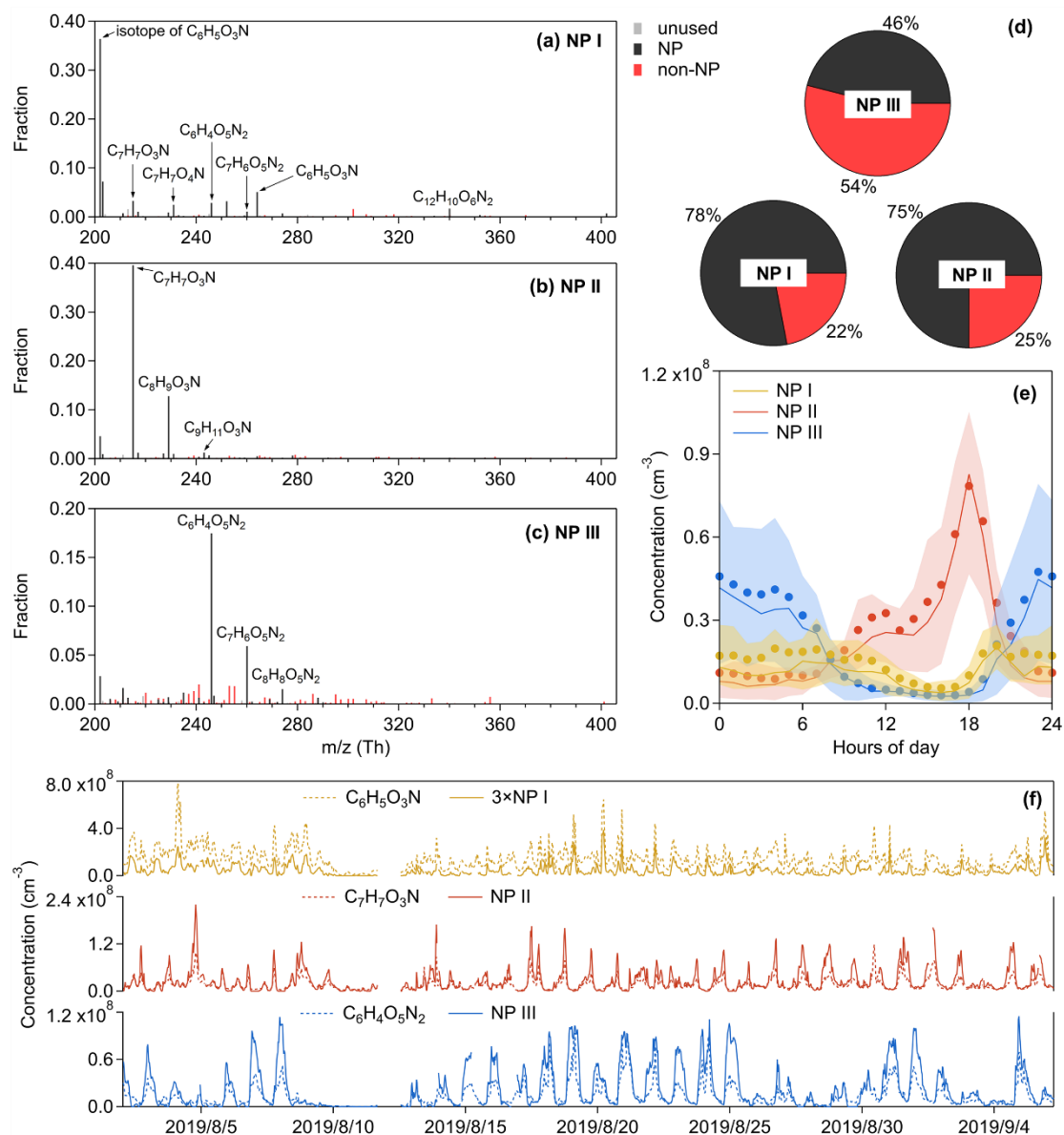
Figure 11. Mass spectra of (a) the NP I factor, (b) the NP II factor, and (c) the NP III factor, and the elemental formulas of major peaks are labeled above them. The gray sticks are fluorinated contaminations, or non-identified compounds. The nitrated phenols are drawn separately with black peaks in (a), (b) and (c), while other OOMs are plotted as red peaks. The molecules represented by the gray were not included in (d). Diurnal patterns of these three factors are shown in (e), the bold solid lines are the median values, shaded areas represent percentiles of 75 % and 25 % and solid circles represent mean values. (f) Time series of PMF factors and tracers.

3.5 Ensemble chemical properties

After performing PMF analysis, over 1000 non-nitro molecules have been identified through HR peaks fitting in each factor. The mean concentration of total non-nitro OOMs reconstructed from the selected PMF solution is about 2.1×10^8 molecules cm^{-3}. Ensemble chemical properties of these non-nitro OOMs are summarized in Fig. 12. The

742 number of carbon atoms implies the precursor information of OOMs. C_5 OOMs, which
743 principally consist of isoprene products benefited from the high reactivity and intensive
744 emissions of isoprene in summer, are the most abundant (Fig. 12(c)). While C_6-C_9
745 OOMs are mostly likely formed from the oxidation of AVOCs such as aromatics and
746 aliphatic series in the urban and suburban atmosphere, and as we expected, these
747 AVOCs-derived OOMs account for about 50% of the total signal (Fig. 12(c)). The
748 intensity of OOMs decreases from C_7 to C_9 determined by the concentration distribution
749 of precursors, but becomes a plateau at C_{10} (Fig. 12(c)), indicating another source of
750 C_{10} OOMs, such as monoterpenes oxidation. These results underscore the formation of
751 SOA precursors from a mixture of anthropogenic and biogenic emissions, under
752 ongoing forest cover increases (Wang et al., 2020a) in highly urbanized eastern China.
753
754 In addition to the anthropogenic VOCs, another human-induced perturbation on the
755 formation of OOMs is the NO_x-affected chemistry of VOCs, i.e., RO_2 + NO
756 terminations or NO_3-iniated oxidations. As showed in Fig. 12(c), about 70% of OOMs
757 are nitrogen-bearing compounds, regarded as organic nitrates within the allowed range
758 of uncertainty. If isoprene nitrates are not included, organic nitrates peak at C_7 as do the
759 nitrogen-free species, showing the significant production of organic nitrates through the
760 AVOCs + NO_x pathways. The NO_x effect on AVOCs-derived OOMs, typified by the
761 Aro-OOMs factor and the Aliph-OOMs factor, are not showed in previous ambient
762 measurements (Yan et al., 2016;Lee et al., 2016;Massoli et al., 2018).
763
764 OOMs grouped by carbon numbers or nitrogen numbers consistently have absolute
765 high concentrations in the daytime (Fig. 12(a) and (b)), revealing the crucial role of
766 photochemical progress, involving RO_2 + NO termination reactions, on OOMs. In
767 addition, The C_5-C_{10} OOMs are enhanced again during 19:00-22:00 LT, and the
768 nighttime peak of C_{10} OOMs is even higher than its daytime peak (Fig. 12(a)). The
769 nocturnal C_{10} OOMs are more intense than C_9 OOMs (Fig. 12(a)), and there are more
770 C_{10} nitrates than C_9 nitrates (Fig. 12(c)). These results show the fate of VOCs degraded
771 by NO_3 during the nighttime, which are more important to monoterpenes. In contrast to
772 nitrogen-free OOMs, organic nitrates are enriched through the reactions of BVOCs with
773 NO_3 in the early evening (Fig. 12(b)), as indicated by three BVOCs nighttime chemistry
774 factors.
775
776 Apart from reflecting the influence of NO_x, multi-nitrates also imply the multiple
777 generations of VOCs oxidation, which is evident in the products of isoprene (e.g.,
778 $C_5H_{10}O_8N_2$ and $C_5H_9O_{10}N_3$) due to its two carbon-carbon double bonds. As products of
779 mononitrates, multi-nitrates follow mononitrates in diurnal variation, with double peaks
780 initiated by OH and NO_3 respectively (Fig. 12(b)). Considering that the formation of
781 organic nitrate is only a small branch of RO_2 + NO termination, the contribution of
782 multi-step oxidation should be larger than that shown in Fig. 12(c).
783
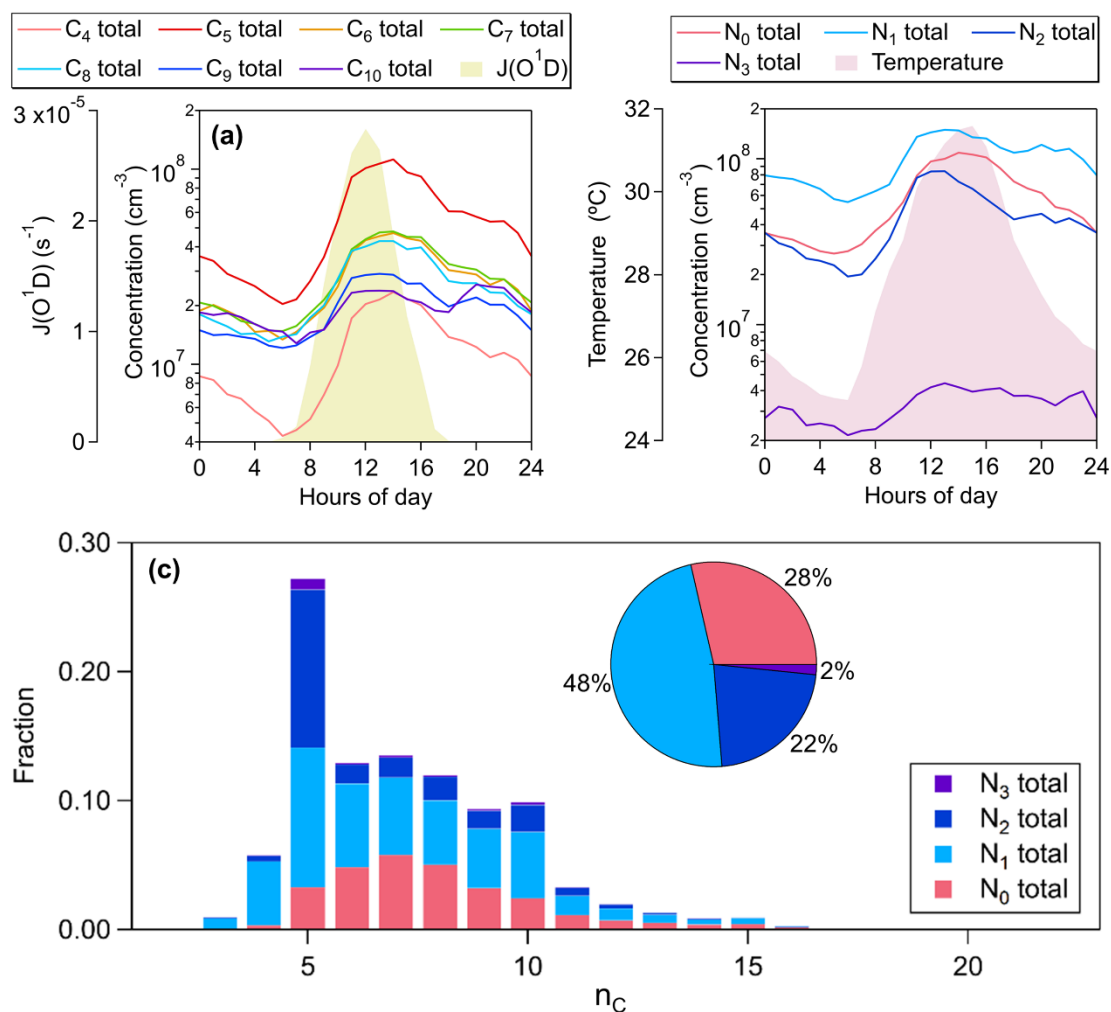
Figure 12. Ensemble chemical properties of non-nitro OOMs reconstructed from the selected PMF solution. (a) Median diurnal cycles of total compounds with carbon number of 5-10 respectively. (b) Median diurnal cycles of total compounds with n_N of 0-3 respectively. (c) The distributions of total observed OOMs at different n_C. OOMs on each carbon number is grouped by nitrogen number, and the total concentration fractions of each groups are reported in the pie chart. Since we selected peaks in the m/z range of 202-404 Th, OOMs with $n_C < 5$ or $n_C > 10$ detected by nitrate CI-APi-TOF are underestimated.

4 Conclusions

We have investigated the sources and characteristics of gas-phase OOMs observed using a nitrate CI-APi-TOF at the SORPES station in the YRD of eastern China, an environment dominated by anthropogenic emissions with enhanced biogenic emissions during summer.

The binPMF analysis, which avoids the uncertainty introduced by high-resolution peak fitting to the input data matrix, was applied to deconvolve the complexity of the data set, and it resolved 14 factors, among which 12 factors have been discussed in detail. A

804 morning factor (Aro-OOMs), correlated with the production rates of RO_2 from
805 aromatics, is characterized by unsaturated products of aromatics such as $C_xH_{2x-5}O_{6-9}N$
806 (x=6-12). An afternoon factor (Aliph-OOMs), containing the bulk of C_6-C_9 dinitrates
807 and trinitrates such as $C_xH_{2x-2}O_8N_2$ (x=4-13) and $C_xH_{2x}O_8N_2$ (x=4-8), is assumed to be
808 derived from aliphatics oxidation. A transported factor (Isop-OOMs), correlates with
809 MVK / MACR and SOA, is exclusively dominated by isoprene nitrates (e.g.,
810 $C_5H_{10}O_8N_2$ and $C_5H_9O_{10}N_3$). A nighttime factor (BVOCs-OOMs III), related to NO, is
811 dominated by terpenes nitrates such as $C_{10}H_{15}O_6N$, $C_{10}H_{16}O_{7-10}N_2$ and $C_{10}H_{17}O_{10}N_3$. In
812 addition to the factors distinguished by precursors, several factors are driven by
813 chemistry. A factor following the $J(O^1D)$ (Photo-related), consisting of isoprene
814 products mixed with others, is thought to be produced by in situ photochemistry. An
815 afternoon factor (Temp-related), having the most abundant nitrogen-free OOMs such
816 as $C_xH_{2x-4}O_{5-6}$ (x=5-10), $C_xH_{2x-2}O_5$ (x=5-10), and $C_xH_{2x-6}O_4$ (x=5-10), is generated
817 involving temperature-influenced chemistry. A daytime factor (O_x & SOA-related),
818 correlated well with O_x and SOA, indicates the photochemical aging process. Two
819 nighttime factors (BVOCs-OOMs I & II), benefiting from NO_3 and suppressed by NO,
820 are considered to be produced from NO_3-iniated oxidation of BVOCs, and both of them
821 have the fingerprint molecule, $C_{10}H_{16}O_9N$. The remaining three factors are governed
822 by nitrated phenols.
823
824 All of these factors from various precursors are influenced in different ways by NO_x.
825 Over 1000 non-nitro molecules have been identified and then reconstructed from
826 selected solution of binPMF, and about 72% of the total signal are contributed by
827 nitrogen-containing OOMs, almost regarded as organic nitrates formed through RO_2 +
828 NO terminations or NO_3-initiated oxidations. Moreover, multi-nitrates have a
829 contribution ratio of about 23% to total concentration, indicating the significant
830 presence of multiple oxidation generations, especially for isoprene (e.g., $C_5H_{10}O_8N_2$
831 and $C_5H_9O_{10}N_3$). The nitrate CI-APi-TOF data set presented here highlight the decisive
832 role of NO_x chemistry on OOMs formation in densely populated areas.
833
834 The differences in OOMs observed in different environments are so clear and the
835 underlying causes are well worth thinking. The precursors, oxidants, and formation
836 pathways of OOMs are changing when moving from urbanized areas to pristine regions,
837 as AVOCs and NOx concentrations decrease, and BVOCs concentrations increase. This
838 process can also occur under the trend of global warming and anthropogenic emissions
839 mitigation, but we still know very little about it. Clarifying the variations of
840 compositions, properties and formation efficiency of OOMs will help to understand the
841 evolution of SOA production during this process. In summary, our findings highlight
842 the dramatic interactions between anthropogenic and biogenic emissions, and
843 encourage more investigations from a mechanistic point of view.
844
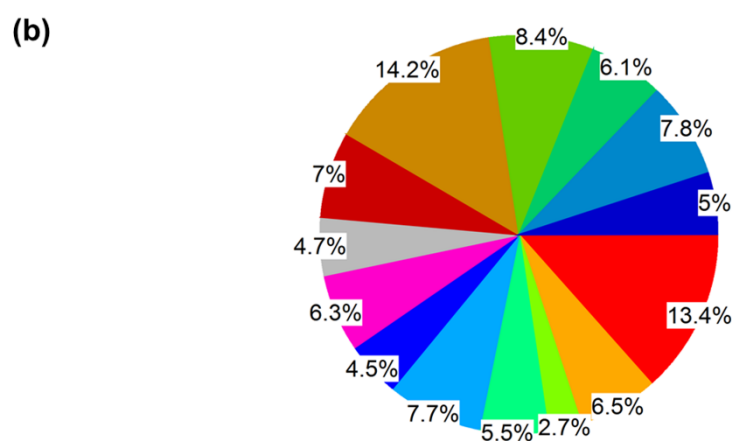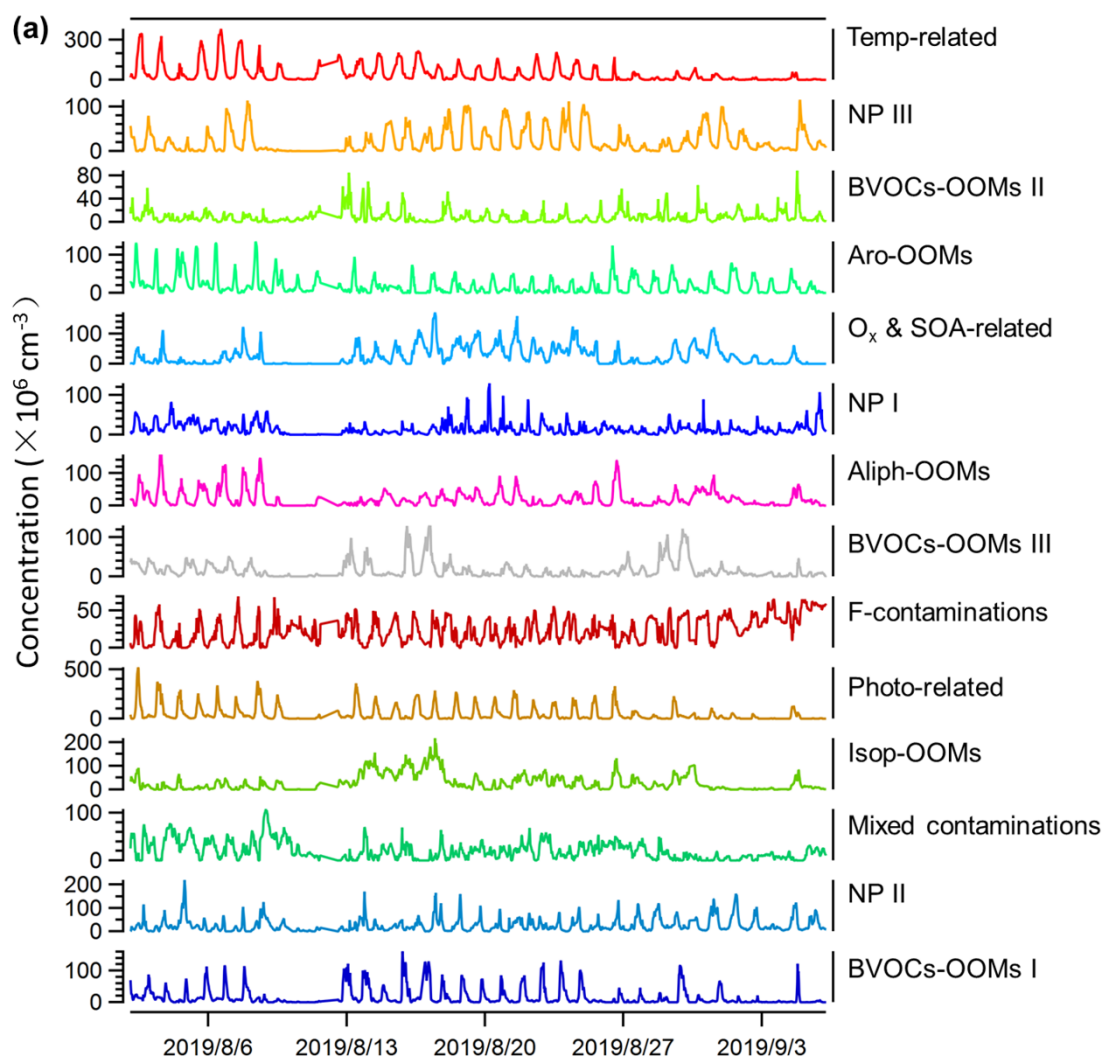845 **Appendix A. The selected solution of binPMF analysis on nitrate CI-APi-TOF data**
846
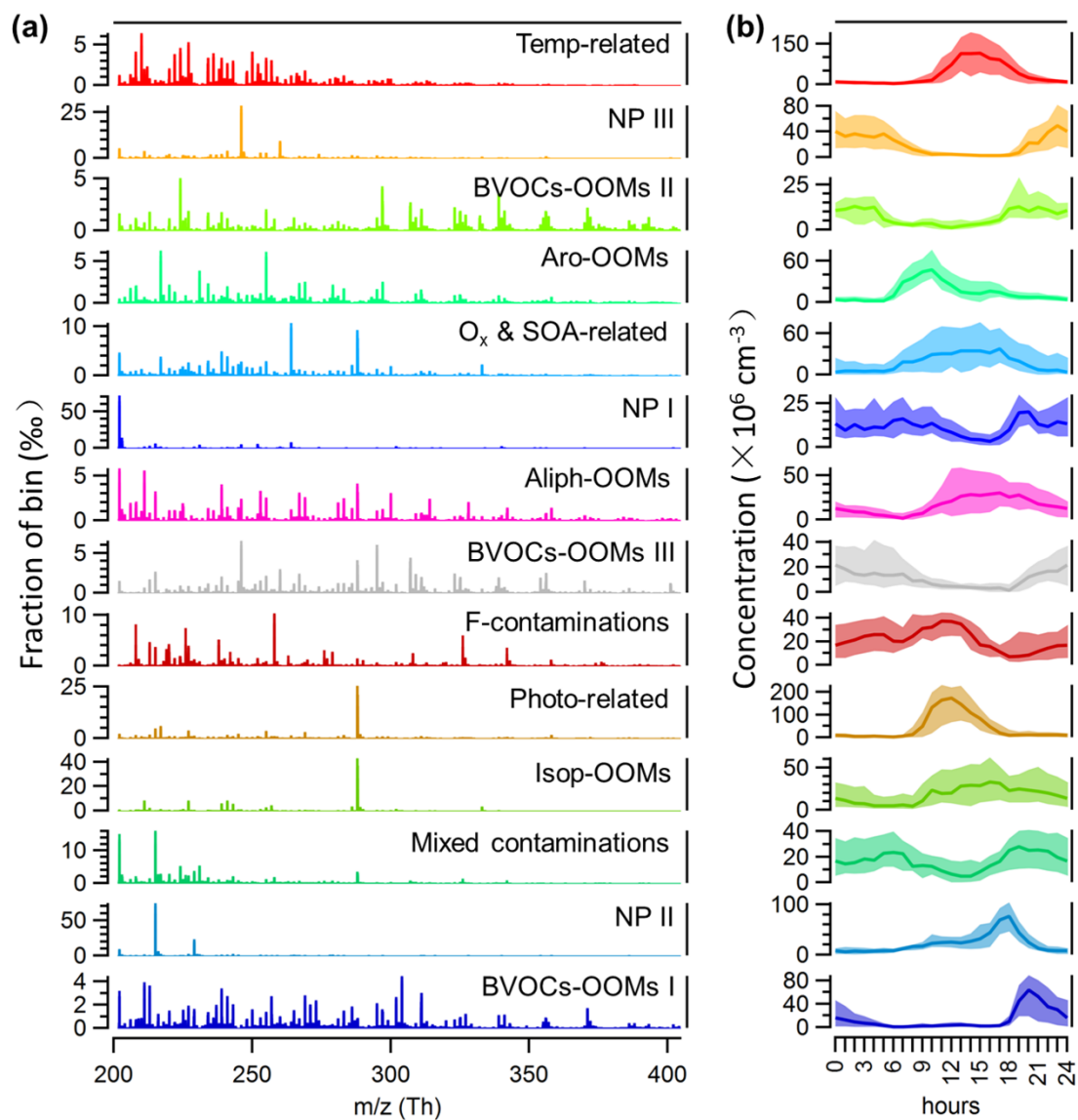
847

848 Figure A1. The selected solution for binPMF analysis of nitrate CI-APi-TOF data,

849 showing (a) mass profile and (b) diurnal cycle of different factor.

850

851

Figure A2. The selected solution for binPMF analysis of nitrate CI-APi-TOF, showing (a) time series of and (b) contribution to total signal reconstructed by PMF of each factor.

Data availability. Measurement data at the SORPES station, including OOMs data and relevant trace gases and aerosol data as well as meteorological data, are available upon

request from the corresponding author before the SORPES database is open to the public.

Author contributions. WN and AD designed this research. YL, YL, DG, CL, ZX, LC, TW, LW, PS, XQ, JW and XC conducted the measurements. YL, WN, CY, YZ, DH, ZW, and DW analyzed the data. YL, WN, ND, ME and AD wrote the paper.

Reference

Atkinson, R.: Atmospheric chemistry of VOCs and NOx, Atmos. Environ., 34, 2063-2101, 10.1016/s1352-2310(99)00460-4, 2000.

Ayres, B. R., Allen, H. M., Draper, D. C., Brown, S. S., Wild, R. J., Jimenez, J. L., Day, D. A., Campuzano-Jost, P., Hu, W., de Gouw, J., Koss, A., Cohen, R. C., Duffey, K. C., Romer, P., Baumann, K., Edgerton, E., Takahama, S., Thornton, J. A., Lee, B. H., Lopez-Hilfiker, F. D., Mohr, C., Wennberg, P. O., Nguyen, T. B., Teng, A., Goldstein, A. H., Olson, K., and Fry, J. L.: Organic nitrate aerosol formation via NO_3 + biogenic volatile organic compounds in the southeastern United States, Atmos. Chem. Phys., 15, 13377-13392, 10.5194/acp-15-13377-2015, 2015.

Beck, L. J., Sarnela, N., Junninen, H., Hoppe, C. J. M., Garmash, O., Bianchi, F., Riva, M., Rose, C., Peräkylä, O., Wimmer, D., Kausiala, O., Jokinen, T., Ahonen, L., Mikkilä, J., Hakala, J., He, X.-C., Kontkanen, J., Wolf, K. K. E., Cappelletti, D., Mazzola, M., Traversi, R., Petroselli, C., Viola, A. P., Vitale, V., Lange, R., Massling, A., Nøjgaard, J. K., Krejci, R., Karlsson, L., Zieger, P., Jang, S., Lee, K., Vakkari, V., Lampilahti, J., Thakur, R. C., Leino, K., Kangasluoma, J., Duplissy, E.-M., Siivola, E., Marbouti, M., Tham, Y. J., Saiz-Lopez, A., Petäjä, T., Ehn, M., Worsnop, D. R., Skov, H., Kulmala, M., Kerminen, V.-M., and Sipilä, M.: Differing mechanisms of new particle formation at two Arctic sites, Geophysical Research Letters, 48, e2020GL091334, https://doi.org/10.1029/2020GL091334, 2021.

Berndt, T., Richters, S., Jokinen, T., Hyttinen, N., Kurten, T., Otkjaer, R. V., Kjaergaard, H. G., Stratmann, F., Herrmann, H., Sipila, M., Kulmala, M., and Ehn, M.: Hydroxyl radical-induced formation of highly oxidized organic compounds, Nature Communications, 7, 10.1038/ncomms13677, 2016.

Bertram, T. H., Kimmel, J. R., Crisp, T. A., Ryder, O. S., Yatavelli, R. L. N., Thornton, J. A., Cubison, M. J., Gonin, M., and Worsnop, D. R.: A field-deployable, chemical ionization time-of-flight mass

902   spectrometer, Atmos. Meas. Tech., 4, 1471-1479, 10.5194/amt-4-1471-2011, 2011.

903   Bianchi, F., Tröstl, J., Junninen, H., Frege, C., Henne, S., Hoyle, C. R., Molteni, U., Herrmann, E.,
904   Adamov, A., Bukowiecki, N., Chen, X., Duplissy, J., Gysel, M., Hutterli, M., Kangasluoma, J.,
905   Kontkanen, J., Kürten, A., Manninen, H. E., Münch, S., Peräkylä, O., Petäjä, T., Rondo, L., Williamson,
906   C., Weingartner, E., Curtius, J., Worsnop, D. R., Kulmala, M., Dommen, J., and Baltensperger, U.: New
907   particle formation in the free troposphere: A question of chemistry and timing, Science, 352, 1109,
908   10.1126/science.aad5456, 2016.

909   Bianchi, F., Kurten, T., Riva, M., Mohr, C., Rissanen, M. P., Roldin, P., Berndt, T., Crounse, J. D.,
910   Wennberg, P. O., Mentel, T. F., Wildt, J., Junninen, H., Jokinen, T., Kulmala, M., Worsnop, D. R.,
911   Thornton, J. A., Donahue, N., Kjaergaard, H. G., and Ehn, M.: Highly oxygenated organic molecules
912   (HOM) from gas-phase autoxidation involving peroxy radicals: a key contributor to atmospheric aerosol,
913   Chem Rev, 10.1021/acs.chemrev.8b00395, 2019.

914   Birdsall, A. W., and Elrod, M. J.: Comprehensive NO-dependent study of the products of the oxidation
915   of atmospherically relevant aromatic compounds, The Journal of Physical Chemistry A, 115, 5397-5407,
916   10.1021/jp2010327, 2011.

917   Bloss, C., Wagner, V., Jenkin, M. E., Volkamer, R., Bloss, W. J., Lee, J. D., Heard, D. E., Wirtz, K.,
918   Martin-Reviejo, M., Rea, G., Wenger, J. C., and Pilling, M. J.: Development of a detailed chemical
919   mechanism (MCMv3.1) for the atmospheric oxidation of aromatic hydrocarbons, Atmospheric
920   Chemistry and Physics, 5, 641-664, 10.5194/acp-5-641-2005, 2005.

921   Calogirou, A., Larsen, B. R., and Kotzias, D.: Gas-phase terpene oxidation products: a review, Atmos.
922   Environ., 33, 1423-1439, https://doi.org/10.1016/S1352-2310(98)00277-5, 1999.

923   Canonaco, F., Crippa, M., Slowik, J. G., Baltensperger, U., and Prévôt, A. S. H.: SoFi, an IGOR-based
924   interface for the efficient use of the generalized multilinear engine (ME-2) for the source apportionment:
925   ME-2 application to aerosol mass spectrometer data, Atmos. Meas. Tech., 6, 3649-3661, 10.5194/amt-6-
926   3649-2013, 2013.

927   Cheng, X., Chen, Q., Li, Y., Huang, G., Liu, Y., Lu, S., Zheng, Y., Qiu, W., Lu, K., Qiu, X., Bianchi, F.,
928   Yan, C., Yuan, B., Shao, M., Wang, Z., Canagaratna, M. R., Zhu, T., Wu, Y., and Zeng, L.: Secondary
929   production of gaseous nitrated phenols in polluted urban environments, Environmental Science &
930   Technology, 55, 4410-4419, 10.1021/acs.est.0c07988, 2021.

931   Crounse, J. D., Nielsen, L. B., Jørgensen, S., Kjaergaard, H. G., and Wennberg, P. O.: Autoxidation of
932   organic compounds in the atmosphere, The Journal of Physical Chemistry Letters, 4, 3513-3520,
933   10.1021/jz4019207, 2013.

934   Desyaterik, Y., Sun, Y., Shen, X., Lee, T., Wang, X., Wang, T., and Collett, J. L.: Speciation of "brown"
935   carbon in cloud water impacted by agricultural biomass burning in eastern China, Journal of Geophysical
936   Research: Atmospheres, 118, 7389-7399, 10.1002/jgrd.50561, 2013.

937   Ding, A., Nie, W., Huang, X., Chi, X., Sun, J., Kerminen, V.-M., Xu, Z., Guo, W., Petäjä, T., Yang, X.,
938   Kulmala, M., and Fu, C.: Long-term observation of air pollution-weather/climate interactions at the
939   SORPES station: a review and outlook, Frontiers of Environmental Science & Engineering, 10, 15,
940   10.1007/s11783-016-0877-3, 2016.

941   Ding, A., Huang, X., Nie, W., Chi, X., Xu, Z., Zheng, L., Xu, Z., Xie, Y., Qi, X., Shen, Y., Sun, P., Wang,
942   J., Wang, L., Sun, J., Yang, X.-Q., Qin, W., Zhang, X., Cheng, W., Liu, W., Pan, L., and Fu, C.: Significant
943   reduction of PM2.5 in eastern China due to regional-scale emission control: evidence from SORPES in
944   2011–2018, Atmospheric Chemistry and Physics, 19, 11791-11801, 10.5194/acp-19-11791-2019, 2019.

945   Ding, A. J., Fu, C. B., Yang, X. Q., Sun, J. N., Zheng, L. F., Xie, Y. N., Herrmann, E., Nie, W., Petäjä, T.,

946 Kerminen, V. M., and Kulmala, M.: Ozone and fine particle in the western Yangtze River Delta: an
947 overview of 1 yr data at the SORPES station, Atmos. Chem. Phys., 13, 5813-5830, 10.5194/acp-13-5813-
948 2013, 2013.

949 Ehn, M., Junninen, H., Petaja, T., Kurten, T., Kerminen, V. M., Schobesberger, S., Manninen, H. E.,
950 Ortega, I. K., Vehkamaki, H., Kulmala, M., and Worsnop, D. R.: Composition and temporal behavior of
951 ambient ions in the boreal forest, Atmospheric Chemistry and Physics, 10, 8513-8530, 10.5194/acp-10-
952 8513-2010, 2010.

953 Ehn, M., Kleist, E., Junninen, H., Petaja, T., Lonn, G., Schobesberger, S., Dal Maso, M., Trimborn, A.,
954 Kulmala, M., Worsnop, D. R., Wahner, A., Wildt, J., and Mentel, T. F.: Gas phase formation of extremely
955 oxidized pinene reaction products in chamber and ambient air, Atmospheric Chemistry and Physics, 12,
956 5113-5127, 10.5194/acp-12-5113-2012, 2012.

957 Ehn, M., Thornton, J. A., Kleist, E., Sipila, M., Junninen, H., Pullinen, I., Springer, M., Rubach, F.,
958 Tillmann, R., Lee, B., Lopez-Hilfiker, F., Andres, S., Acir, I. H., Rissanen, M., Jokinen, T., Schobesberger,
959 S., Kangasluoma, J., Kontkanen, J., Nieminen, T., Kurten, T., Nielsen, L. B., Jorgensen, S., Kjaergaard,
960 H. G., Canagaratna, M., Maso, M. D., Berndt, T., Petaja, T., Wahner, A., Kerminen, V. M., Kulmala, M.,
961 Worsnop, D. R., Wildt, J., and Mentel, T. F.: A large source of low-volatility secondary organic aerosol,
962 Nature, 506, 476-479, 10.1038/nature13032, 2014.

963 Faxon, C., Hammes, J., Le Breton, M., Pathak, R. K., and Hallquist, M.: Characterization of organic
964 nitrate constituents of secondary organic aerosol (SOA) from nitrate-radical-initiated oxidation of
965 limonene using high-resolution chemical ionization mass spectrometry, Atmos. Chem. Phys., 18, 5467-
966 5481, 10.5194/acp-18-5467-2018, 2018.

967 Finlayson-Pitts, B. J., and Pitts, J. N.: CHAPTER 8 - Acid Deposition: Formation and Fates of Inorganic
968 and Organic Acids in the Troposphere, in: Chemistry of the Upper and Lower Atmosphere, edited by:
969 Finlayson-Pitts, B. J., and Pitts, J. N., Academic Press, San Diego, 294-348, 2000.

970 Frege, C., Ortega, I. K., Rissanen, M. P., Praplan, A. P., Steiner, G., Heinritzi, M., Ahonen, L., Amorim,
971 A., Bernhammer, A.-K., Bianchi, F., Brilke, S., Breitenlechner, M., Dada, L., Dias, A., Duplissy, J.,
972 Ehrhart, S., El-Haddad, I., Fischer, L., Fuchs, C., Garmash, O., Gonin, M., Hansel, A., Hoyle, C. R.,
973 Jokinen, T., Junninen, H., Kirkby, J., Kürten, A., Lehtipalo, K., Leiminger, M., Mauldin, R. L., Molteni,
974 U., Nichman, L., Petäjä, T., Sarnela, N., Schobesberger, S., Simon, M., Sipilä, M., Stolzenburg, D., Tomé,
975 A., Vogel, A. L., Wagner, A. C., Wagner, R., Xiao, M., Yan, C., Ye, P., Curtius, J., Donahue, N. M., Flagan,
976 R. C., Kulmala, M., Worsnop, D. R., Winkler, P. M., Dommen, J., and Baltensperger, U.: Influence of
977 temperature on the molecular composition of ions and charged clusters during pure biogenic nucleation,
978 Atmospheric Chemistry and Physics, 18, 65-79, 10.5194/acp-18-65-2018, 2018.

979 Fu, X., Wang, S. X., Zhao, B., Xing, J., Cheng, Z., Liu, H., and Hao, J. M.: Emission inventory of primary
980 pollutants and chemical speciation in 2010 for the Yangtze River Delta region, China, Atmos. Environ.,
981 70, 39-50, 10.1016/j.atmosenv.2012.12.034, 2013.

982 Fuchs, N. A., and Sutugin, A. G.: High-Dispersed Aerosols, in: Topics in Current Aerosol Research,
983 edited by: Hidy, G. M., and Brock, J. R., Pergamon, 1, 1971.

984 Garmash, O., Rissanen, M. P., Pullinen, I., Schmitt, S., Kausiala, O., Tillmann, R., Zhao, D., Percival, C.,
985 Bannan, T. J., Priestley, M., Hallquist, Å. M., Kleist, E., Kiendler-Scharr, A., Hallquist, M., Berndt, T.,
986 McFiggans, G., Wildt, J., Mentel, T. F., and Ehn, M.: Multi-generation OH oxidation as a source for
987 highly oxygenated organic molecules from aromatics, Atmospheric Chemistry and Physics, 20, 515-537,
988 10.5194/acp-20-515-2020, 2020.

989 Guo, Y., Yan, C., Li, C., Ma, W., Feng, Z., Zhou, Y., Lin, Z., Dada, L., Stolzenburg, D., Yin, R., Kontkanen,

J., Daellenbach, K. R., Kangasluoma, J., Yao, L., Chu, B., Wang, Y., Cai, R., Bianchi, F., Liu, Y., and Kulmala, M.: Formation of nighttime sulfuric acid from the ozonolysis of alkenes in Beijing, Atmos. Chem. Phys., 21, 5499-5511, 10.5194/acp-21-5499-2021, 2021.

Hallquist, M., Wenger, J. C., Baltensperger, U., Rudich, Y., Simpson, D., Claeys, M., Dommen, J., Donahue, N. M., George, C., Goldstein, A. H., Hamilton, J. F., Herrmann, H., Hoffmann, T., Iinuma, Y., Jang, M., Jenkin, M. E., Jimenez, J. L., Kiendler-Scharr, A., Maenhaut, W., McFiggans, G., Mentel, T. F., Monod, A., Prevot, A. S. H., Seinfeld, J. H., Surratt, J. D., Szmigielski, R., and Wildt, J.: The formation, properties and impact of secondary organic aerosol: current and emerging issues, Atmospheric Chemistry and Physics, 9, 5155-5236, 10.5194/acp-9-5155-2009, 2009.

Harrison, M. A. J., Barra, S., Borghesi, D., Vione, D., Arsene, C., and Iulian Olariu, R.: Nitrated phenols in the atmosphere: a review, Atmos. Environ., 39, 231-248, https://doi.org/10.1016/j.atmosenv.2004.09.044, 2005.

Heinritzi, M., Simon, M., Steiner, G., Wagner, A. C., Kuerten, A., Hansel, A., and Curtius, J.: Characterization of the mass-dependent transmission efficiency of a CIMS, Atmospheric Measurement Techniques, 9, 1449-1460, 10.5194/amt-9-1449-2016, 2016.

Heinritzi, M., Dada, L., Simon, M., Stolzenburg, D., Wagner, A. C., Fischer, L., Ahonen, L. R., Amanatidis, S., Baalbaki, R., Baccarini, A., Bauer, P. S., Baumgartner, B., Bianchi, F., Brilke, S., Chen, D., Chiu, R., Dias, A., Dommen, J., Duplissy, J., Finkenzeller, H., Frege, C., Fuchs, C., Garmash, O., Gordon, H., Granzin, M., El Haddad, I., He, X., Helm, J., Hofbauer, V., Hoyle, C. R., Kangasluoma, J., Keber, T., Kim, C., Kürten, A., Lamkaddam, H., Laurila, T. M., Lampilahti, J., Lee, C. P., Lehtipalo, K., Leiminger, M., Mai, H., Makhmutov, V., Manninen, H. E., Marten, R., Mathot, S., Mauldin, R. L., Mentler, B., Molteni, U., Müller, T., Nie, W., Nieminen, T., Onnela, A., Partoll, E., Passananti, M., Petäjä, T., Pfeifer, J., Pospisilova, V., Quéléver, L. L. J., Rissanen, M. P., Rose, C., Schobesberger, S., Scholz, W., Scholze, K., Sipilä, M., Steiner, G., Stozhkov, Y., Tauber, C., Tham, Y. J., Vazquez-Pufleau, M., Virtanen, A., Vogel, A. L., Volkamer, R., Wagner, R., Wang, M., Weitz, L., Wimmer, D., Xiao, M., Yan, C., Ye, P., Zha, Q., Zhou, X., Amorim, A., Baltensperger, U., Hansel, A., Kulmala, M., Tomé, A., Winkler, P. M., Worsnop, D. R., Donahue, N. M., Kirkby, J., and Curtius, J.: Molecular understanding of the suppression of new-particle formation by isoprene, Atmos. Chem. Phys., 20, 11809-11821, 10.5194/acp-20-11809-2020, 2020.

Herndon, S. C., Onasch, T. B., Wood, E. C., Kroll, J. H., Canagaratna, M. R., Jayne, J. T., Zavala, M. A., Knighton, W. B., Mazzoleni, C., Dubey, M. K., Ulbrich, I. M., Jimenez, J. L., Seila, R., de Gouw, J. A., de Foy, B., Fast, J., Molina, L. T., Kolb, C. E., and Worsnop, D. R.: Correlation of secondary organic aerosol with odd oxygen in Mexico City, Geophysical Research Letters, 35, 10.1029/2008gl034058, 2008.

Hu, W., Hu, M., Hu, W., Jimenez, J. L., Yuan, B., Chen, W., Wang, M., Wu, Y., Chen, C., Wang, Z., Peng, J., Zeng, L., and Shao, M.: Chemical composition, sources, and aging process of submicron aerosols in Beijing: Contrast between summer and winter, Journal of Geophysical Research: Atmospheres, 121, 1955-1977, 10.1002/2015jd024020, 2016.

Huang, R. J., Zhang, Y. L., Bozzetti, C., Ho, K. F., Cao, J. J., Han, Y. M., Daellenbach, K. R., Slowik, J. G., Platt, S. M., Canonaco, F., Zotter, P., Wolf, R., Pieber, S. M., Bruns, E. A., Crippa, M., Ciarelli, G., Piazzalunga, A., Schwikowski, M., Abbaszade, G., Schnelle-Kreis, J., Zimmermann, R., An, Z. S., Szidat, S., Baltensperger, U., El Haddad, I., and Prevot, A. S. H.: High secondary aerosol contribution to particulate pollution during haze events in China, Nature, 514, 218-222, 10.1038/nature13774, 2014.

Hyttinen, N., Kupiainen-Määttä, O., Rissanen, M. P., Muuronen, M., Ehn, M., and Kurtén, T.: Modeling

the Charging of Highly Oxidized Cyclohexene Ozonolysis Products Using Nitrate-Based Chemical Ionization, The Journal of Physical Chemistry A, 119, 6339-6345, 10.1021/acs.jpca.5b01818, 2015.

Intergovernmental Panel on Climate, C.: Climate Change 2013 – The physical science basis: working group I contribution to the fifth assessment report of the Intergovernmental Panel on Climate Change, Cambridge University Press, Cambridge, 2014.

Jenkin, M. E., Young, J. C., and Rickard, A. R.: The MCM v3.3.1 degradation scheme for isoprene, Atmos. Chem. Phys., 15, 11433-11459, 10.5194/acp-15-11433-2015, 2015.

Jimenez, J. L., Canagaratna, M. R., Donahue, N. M., Prevot, A. S. H., Zhang, Q., Kroll, J. H., DeCarlo, P. F., Allan, J. D., Coe, H., Ng, N. L., Aiken, A. C., Docherty, K. S., Ulbrich, I. M., Grieshop, A. P., Robinson, A. L., Duplissy, J., Smith, J. D., Wilson, K. R., Lanz, V. A., Hueglin, C., Sun, Y. L., Tian, J., Laaksonen, A., Raatikainen, T., Rautiainen, J., Vaattovaara, P., Ehn, M., Kulmala, M., Tomlinson, J. M., Collins, D. R., Cubison, M. J., Dunlea, E. J., Huffman, J. A., Onasch, T. B., Alfarra, M. R., Williams, P. I., Bower, K., Kondo, Y., Schneider, J., Drewnick, F., Borrmann, S., Weimer, S., Demerjian, K., Salcedo, D., Cottrell, L., Griffin, R., Takami, A., Miyoshi, T., Hatakeyama, S., Shimono, A., Sun, J. Y., Zhang, Y. M., Dzepina, K., Kimmel, J. R., Sueper, D., Jayne, J. T., Herndon, S. C., Trimborn, A. M., Williams, L. R., Wood, E. C., Middlebrook, A. M., Kolb, C. E., Baltensperger, U., and Worsnop, D. R.: Evolution of organic aerosols in the atmosphere, Science, 326, 1525-1529, 10.1126/science.1180353, 2009.

Jokinen, T., Sipila, M., Junninen, H., Ehn, M., Lonn, G., Hakala, J., Petaja, T., Mauldin, R. L., III, Kulmala, M., and Worsnop, D. R.: Atmospheric sulphuric acid and neutral cluster measurements using CI-APi-TOF, Atmospheric Chemistry and Physics, 12, 4117-4125, 10.5194/acp-12-4117-2012, 2012.

Jokinen, T., Sipila, M., Richters, S., Kerminen, V. M., Paasonen, P., Stratmann, F., Worsnop, D., Kulmala, M., Ehn, M., Herrmann, H., and Berndt, T.: Rapid autoxidation forms highly oxidized RO_2 radicals in the atmosphere, Angew. Chem.-Int. Edit., 53, 14596-14600, 10.1002/anie.201408566, 2014.

Jokinen, T., Berndt, T., Makkonen, R., Kerminen, V. M., Junninen, H., Paasonen, P., Stratmann, F., Herrmann, H., Guenther, A. B., Worsnop, D. R., Kulmala, M., Ehn, M., and Sipila, M.: Production of extremely low volatile organic compounds from biogenic emissions: Measured yields and atmospheric implications, Proc Natl Acad Sci U S A, 112, 7123-7128, 10.1073/pnas.1423977112, 2015.

Junninen, H., Ehn, M., Petaja, T., Luosujarvi, L., Kotiaho, T., Kostiainen, R., Rohner, U., Gonin, M., Fuhrer, K., Kulmala, M., and Worsnop, D. R.: A high-resolution mass spectrometer to measure atmospheric ion composition, Atmospheric Measurement Techniques, 3, 1039-1053, 10.5194/amt-3-1039-2010, 2010.

Karl, T., Striednig, M., Graus, M., Hammerle, A., and Wohlfahrt, G.: Urban flux measurements reveal a large pool of oxygenated volatile organic compound emissions, Proceedings of the National Academy of Sciences, 115, 1186, 10.1073/pnas.1714715115, 2018.

Kirkby, J., Duplissy, J., Sengupta, K., Frege, C., Gordon, H., Williamson, C., Heinritzi, M., Simon, M., Yan, C., Almeida, J., Trostl, J., Nieminen, T., Ortega, I. K., Wagner, R., Adamov, A., Amorim, A., Bernhammer, A. K., Bianchi, F., Breitenlechner, M., Brilke, S., Chen, X. M., Craven, J., Dias, A., Ehrhart, S., Flagan, R. C., Franchin, A., Fuchs, C., Guida, R., Hakala, J., Hoyle, C. R., Jokinen, T., Junninen, H., Kangasluoma, J., Kim, J., Krapf, M., Kurten, A., Laaksonen, A., Lehtipalo, K., Makhmutov, V., Mathot, S., Molteni, U., Onnela, A., Perakyla, O., Piel, F., Petaja, T., Praplan, A. P., Pringle, K., Rap, A., Richards, N. A. D., Riipinen, I., Rissanen, M. P., Rondo, L., Sarnela, N., Schobesberger, S., Scott, C. E., Seinfeld, J. H., Sipila, M., Steiner, G., Stozhkov, Y., Stratmann, F., Tome, A., Virtanen, A., Vogel, A. L., Wagner, A. C., Wagner, P. E., Weingartner, E., Wimmer, D., Winkler, P. M., Ye, P. L., Zhang, X., Hansel, A., Dommen, J., Donahue, N. M., Worsnop, D. R., Baltensperger, U., Kulmala, M., Carslaw, K. S., and

1078   Curtius, J.: Ion-induced nucleation of pure biogenic particles, Nature, 533, 521-+, 10.1038/nature17953,
1079   2016.

1080   Kuerten, A., Rondo, L., Ehrhart, S., and Curtius, J.: Calibration of a chemical ionization mass
1081   spectrometer for the measurement of gaseous sulfuric acid, J. Phys. Chem. A, 116, 6375-6386,
1082   10.1021/jp212123n, 2012.

1083   Kulmala, M., Petaja, T., Nieminen, T., Sipila, M., Manninen, H. E., Lehtipalo, K., Dal Maso, M., Aalto,
1084   P. P., Junninen, H., Paasonen, P., Riipinen, I., Lehtinen, K. E., Laaksonen, A., and Kerminen, V. M.:
1085   Measurement of the nucleation of atmospheric aerosol particles, Nat Protoc, 7, 1651-1667,
1086   10.1038/nprot.2012.091, 2012.

1087   Kulmala, M., Kontkanen, J., Junninen, H., Lehtipalo, K., Manninen, H. E., Nieminen, T., Petaja, T., Sipila,
1088   M., Schobesberger, S., Rantala, P., Franchin, A., Jokinen, T., Jarvinen, E., Aijala, M., Kangasluoma, J.,
1089   Hakala, J., Aalto, P. P., Paasonen, P., Mikkila, J., Vanhanen, J., Aalto, J., Hakola, H., Makkonen, U.,
1090   Ruuskanen, T., Mauldin, R. L., III, Duplissy, J., Vehkamaki, H., Back, J., Kortelainen, A., Riipinen, I.,
1091   Kurten, T., Johnston, M. V., Smith, J. N., Ehn, M., Mentel, T. F., Lehtinen, K. E. J., Laaksonen, A.,
1092   Kerminen, V.-M., and Worsnop, D. R.: Direct observations of atmospheric aerosol nucleation, Science,
1093   339, 943-946, 10.1126/science.1227385, 2013.

1094   Kwan, A. J., Chan, A. W. H., Ng, N. L., Kjaergaard, H. G., Seinfeld, J. H., and Wennberg, P. O.: Peroxy
1095   radical chemistry and OH radical production during the NO_3-initiated oxidation of isoprene, Atmos.
1096   Chem. Phys., 12, 7499-7515, 10.5194/acp-12-7499-2012, 2012.

1097   Lambe, A., Massoli, P., Zhang, X., Canagaratna, M., Nowak, J., Daube, C., Yan, C., Nie, W., Onasch, T.,
1098   Jayne, J., Kolb, C., Davidovits, P., Worsnop, D., and Brune, W.: Controlled nitric oxide production via
1099 $O(1D) + N_2O$ reactions for use in oxidation flow reactor studies, Atmos. Meas. Tech., 10, 2283-2298,
1100   10.5194/amt-10-2283-2017, 2017.

1101   Lee, B. H., Lopez-Hilfiker, F. D., Mohr, C., Kurtén, T., Worsnop, D. R., and Thornton, J. A.: An iodide-
1102   adduct high-resolution time-of-flight chemical-ionization mass spectrometer: application to atmospheric
1103   inorganic and organic compounds, Environmental Science & Technology, 48, 6309-6317,
1104   10.1021/es500362a, 2014.

1105   Lee, B. H., Mohr, C., Lopez-Hilfiker, F. D., Lutz, A., Hallquist, M., Lee, L., Romer, P., Cohen, R. C.,
1106   Iyer, S., Kurtén, T., Hu, W., Day, D. A., Campuzano-Jost, P., Jimenez, J. L., Xu, L., Ng, N. L., Guo, H.,
1107   Weber, R. J., Wild, R. J., Brown, S. S., Koss, A., de Gouw, J., Olson, K., Goldstein, A. H., Seco, R., Kim,
1108   S., McAvey, K., Shepson, P. B., Starn, T., Baumann, K., Edgerton, E. S., Liu, J., Shilling, J. E., Miller,
1109   D. O., Brune, W., Schobesberger, S., Ambro, E. L., and Thornton, J. A.: Highly functionalized organic
1110   nitrates in the southeast United States: Contribution to secondary organic aerosol and reactive nitrogen
1111   budgets, Proceedings of the National Academy of Sciences, 113, 1516, 10.1073/pnas.1508108113, 2016.

1112   Li, Y., Nie, W., Liu, Y., Huang, D., Xu, Z., Peng, X., George, C., Yan, C., Tham, Y. J., Yu, C., Xia, M.,
1113   Fu, X., Wang, X., Xue, L., Wang, Z., Xu, Z., Chi, X., Wang, T., and Ding, A.: Photoinduced production
1114   of chlorine molecules from titanium dioxide surfaces containing chloride, Environmental Science &
1115   Technology Letters, 7, 70-75, 10.1021/acs.estlett.9b00704, 2020.

1116   Lim, S. S., Vos, T., Flaxman, A. D., Danaei, G., Shibuya, K., Adair-Rohani, H., Amann, M., Anderson,
1117   H. R., Andrews, K. G., Aryee, M., Atkinson, C., Bacchus, L. J., Bahalim, A. N., Balakrishnan, K., Balmes,
1118   J., Barker-Collo, S., Baxter, A., Bell, M. L., Blore, J. D., Blyth, F., Bonner, C., Borges, G., Bourne, R.,
1119   Boussinesq, M., Brauer, M., Brooks, P., Bruce, N. G., Brunekreef, B., Bryan-Hancock, C., Bucello, C.,
1120   Buchbinder, R., Bull, F., Burnett, R. T., Byers, T. E., Calabria, B., Carapetis, J., Carnahan, E., Chafe, Z.,
1121   Charlson, F., Chen, H. L., Chen, J. S., Cheng, A. T. A., Child, J. C., Cohen, A., Colson, K. E., Cowie, B.

C., Darby, S., Darling, S., Davis, A., Degenhardt, L., Dentener, F., Des Jarlais, D. C., Devries, K., Dherani, M., Ding, E. L., Dorsey, E. R., Driscoll, T., Edmond, K., Ali, S. E., Engell, R. E., Erwin, P. J., Fahimi, S., Falder, G., Farzadfar, F., Ferrari, A., Finucane, M. M., Flaxman, S., Fowkes, F. G. R., Freedman, G., Freeman, M. K., Gakidou, E., Ghosh, S., Giovannucci, E., Gmel, G., Graham, K., Grainger, R., Grant, B., Gunnell, D., Gutierrez, H. R., Hall, W., Hoek, H. W., Hogan, A., Hosgood, H. D., Hoy, D., Hu, H., Hubbell, B. J., Hutchings, S. J., Ibeanusi, S. E., Jacklyn, G. L., Jasrasaria, R., Jonas, J. B., Kan, H. D., Kanis, J. A., Kassebaum, N., Kawakami, N., Khang, Y. H., Khatibzadeh, S., Khoo, J. P., Kok, C., Laden, F., Lalloo, R., Lan, Q., Lathlean, T., Leasher, J. L., Leigh, J., Li, Y., Lin, J. K., Lipshultz, S. E., London, S., Lozano, R., Lu, Y., Mak, J., Malekzadeh, R., Mallinger, L., Marcenes, W., March, L., Marks, R., Martin, R., McGale, P., McGrath, J., Mehta, S., Mensah, G. A., Merriman, T. R., Micha, R., Michaud, C., Mishra, V., Hanafiah, K. M., Mokdad, A. A., Morawska, L., Mozaffarian, D., Murphy, T., Naghavi, M., Neal, B., Nelson, P. K., Nolla, J. M., Norman, R., Olives, C., Omer, S. B., Orchard, J., Osborne, R., Ostro, B., Page, A., Pandey, K. D., Parry, C. D. H., Passmore, E., Patra, J., Pearce, N., Pelizzari, P. M., Petzold, M., Phillips, M. R., Pope, D., Pope, C. A., Powles, J., Rao, M., Razavi, H., Rehfuess, E. A., Rehm, J. T., Ritz, B., Rivara, F. P., Roberts, T., Robinson, C., Rodriguez-Portales, J. A., Romieu, I., Room, R., Rosenfeld, L. C., Roy, A., Rushton, L., Salomon, J. A., Sampson, U., Sanchez-Riera, L., Sanman, E., Sapkota, A., Seedat, S., Shi, P. L., Shield, K., Shivakoti, R., Singh, G. M., Sleet, D. A., Smith, E., Smith, K. R., Stapelberg, N. J. C., Steenland, K., Stockl, H., Stovner, L. J., Straif, K., Straney, L., Thurston, G. D., Tran, J. H., Van Dingenen, R., van Donkelaar, A., Veerman, J. L., Vijayakumar, L., Weintraub, R., Weissman, M. M., White, R. A., Whiteford, H., Wiersma, S. T., Wilkinson, J. D., Williams, H. C., Williams, W., Wilson, N., Woolf, A. D., Yip, P., Zielinski, J. M., Lopez, A. D., Murray, C. J. L., and Ezzati, M.: A comparative risk assessment of burden of disease and injury attributable to 67 risk factors and risk factor clusters in 21 regions, 1990-2010: a systematic analysis for the Global Burden of Disease Study 2010, Lancet, 380, 2224-2260, 10.1016/s0140-6736(12)61766-8, 2012.

Liu, Y., Nie, W., Xu, Z., Wang, T., Wang, R., Li, Y., Wang, L., Chi, X., and Ding, A.: Semi-quantitative understanding of source contribution to nitrous acid (HONO) based on 1 year of continuous observation at the SORPES station in eastern China, Atmos. Chem. Phys., 19, 13289-13308, 10.5194/acp-19-13289-2019, 2019.

Lu, Y., Yan, C., Fu, Y., Chen, Y., Liu, Y., Yang, G., Wang, Y., Bianchi, F., Chu, B., Zhou, Y., Yin, R., Baalbaki, R., Garmash, O., Deng, C., Wang, W., Liu, Y., Petäjä, T., Kerminen, V.-M., Jiang, J., Kulmala, M., and Wang, L.: A proxy for atmospheric daytime gaseous sulfuric acid concentration in urban Beijing, Atmospheric Chemistry and Physics, 19, 1971-1983, 10.5194/acp-19-1971-2019, 2019.

Massoli, P., Stark, H., Canagaratna, M. R., Krechmer, J. E., Xu, L., Ng, N. L., Mauldin, R. L., III, Yan, C., Kimmel, J., Misztal, P. K., Jimenez, J. L., Jayne, J. T., and Worsnop, D. R.: Ambient Measurements of Highly Oxidized Gas-Phase Molecules during the Southern Oxidant and Aerosol Study (SOAS) 2013, Acs Earth and Space Chemistry, 2, 653-672, 10.1021/acsearthspacechem.8b00028, 2018.

Mauldin Iii, R. L., Berndt, T., Sipilä, M., Paasonen, P., Petäjä, T., Kim, S., Kurtén, T., Stratmann, F., Kerminen, V. M., and Kulmala, M.: A new atmospherically relevant oxidant of sulphur dioxide, Nature, 488, 193-196, 10.1038/nature11278, 2012.

McFiggans, G., Mentel, T. F., Wildt, J., Pullinen, I., Kang, S., Kleist, E., Schmitt, S., Springer, M., Tillmann, R., Wu, C., Zhao, D., Hallquist, M., Faxon, C., Le Breton, M., Hallquist, A. M., Simpson, D., Bergstrom, R., Jenkin, M. E., Ehn, M., Thornton, J. A., Alfarra, M. R., Bannan, T. J., Percival, C. J., Priestley, M., Topping, D., and Kiendler-Scharr, A.: Secondary organic aerosol reduced by mixture of atmospheric vapours, Nature, 565, 587-593, 10.1038/s41586-018-0871-y, 2019.

Mehra, A., Wang, Y., Krechmer, J. E., Lambe, A., Majluf, F., Morris, M. A., Priestley, M., Bannan, T. J., Bryant, D. J., Pereira, K. L., Hamilton, J. F., Rickard, A. R., Newland, M. J., Stark, H., Croteau, P., Jayne, J. T., Worsnop, D. R., Canagaratna, M. R., Wang, L., and Coe, H.: Evaluation of the chemical composition of gas- and particle-phase products of aromatic oxidation, Atmospheric Chemistry and Physics, 20, 9783-9803, 10.5194/acp-20-9783-2020, 2020.

Mohr, C., Lopez-Hilfiker, F. D., Zotter, P., Prevot, A. S., Xu, L., Ng, N. L., Herndon, S. C., Williams, L. R., Franklin, J. P., Zahniser, M. S., Worsnop, D. R., Knighton, W. B., Aiken, A. C., Gorkowski, K. J., Dubey, M. K., Allan, J. D., and Thornton, J. A.: Contribution of nitrated phenols to wood burning brown carbon light absorption in Detling, United Kingdom during winter time, Environ Sci Technol, 47, 6316-6324, 10.1021/es400683v, 2013.

Molteni, U., Bianchi, F., Klein, F., El Haddad, I., Frege, C., Rossi, M. J., Dommen, J., and Baltensperger, U.: Formation of highly oxygenated organic molecules from aromatic compounds, Atmospheric Chemistry and Physics, 18, 1909-1921, 10.5194/acp-18-1909-2018, 2018.

Nah, T., Sanchez, J., Boyd, C. M., and Ng, N. L.: Photochemical aging of α-pinene and β-pinene secondary organic aerosol formed from nitrate radical oxidation, Environmental Science & Technology, 50, 222-231, 10.1021/acs.est.5b04594, 2016.

Nel, A.: Air pollution-related illness: Effects of particles, Science, 308, 804-806, 10.1126/science.1108752, 2005.

Newland, M. J., Bryant, D. J., Dunmore, R. E., Bannan, T. J., Acton, W. J. F., Langford, B., Hopkins, J. R., Squires, F. A., Dixon, W., Drysdale, W. S., Ivatt, P. D., Evans, M. J., Edwards, P. M., Whalley, L. K., Heard, D. E., Slater, E. J., Woodward-Massey, R., Ye, C., Mehra, A., Worrall, S. D., Bacak, A., Coe, H., Percival, C. J., Hewitt, C. N., Lee, J. D., Cui, T., Surratt, J. D., Wang, X., Lewis, A. C., Rickard, A. R., and Hamilton, J. F.: Low-NO atmospheric oxidation pathways in a polluted megacity, Atmos. Chem. Phys., 21, 1613-1625, 10.5194/acp-21-1613-2021, 2021.

Ng, N. L., Kwan, A. J., Surratt, J. D., Chan, A. W. H., Chhabra, P. S., Sorooshian, A., Pye, H. O. T., Crounse, J. D., Wennberg, P. O., Flagan, R. C., and Seinfeld, J. H.: Secondary organic aerosol (SOA) formation from reaction of isoprene with nitrate radicals (NO_3), Atmospheric Chemistry and Physics, 8, 4117-4140, 10.5194/acp-8-4117-2008, 2008.

Nie, W., Ding, A. J., Xie, Y. N., Xu, Z., Mao, H., Kerminen, V. M., Zheng, L. F., Qi, X. M., Huang, X., Yang, X. Q., Sun, J. N., Herrmann, E., Petäjä, T., Kulmala, M., and Fu, C. B.: Influence of biomass burning plumes on HONO chemistry in eastern China, Atmospheric Chemistry and Physics, 15, 1147-1159, 10.5194/acp-15-1147-2015, 2015.

Orlando, J. J., Tyndall, G. S., and Wallington, T. J.: The atmospheric chemistry of alkoxy radicals, Chemical Reviews, 103, 4657-4689, 10.1021/cr020527p, 2003.

Orlando, J. J., and Tyndall, G. S.: Laboratory studies of organic peroxy radical chemistry: an overview with emphasis on recent issues of atmospheric significance, Chemical Society Reviews, 41, 6294-6317, 10.1039/c2cs35166h, 2012.

Paatero, P., and Tapper, U.: Positve matrix factorization - a nonnegative factor model with optimal utilization of error-estimates of data values, Environmetrics, 5, 111-126, 10.1002/env.3170050203, 1994.

Pye, H. O. T., D'Ambro, E. L., Lee, B., Schobesberger, S., Takeuchi, M., Zhao, Y., Lopez-Hilfiker, F., Liu, J. M., Shilling, J. E., Xing, J., Mathur, R., Middlebrook, A. M., Liao, J., Welti, A., Graus, M., Warneke, C., de Gouw, J. A., Holloway, J. S., Ryerson, T. B., Pollack, I. B., and Thornton, J. A.: Anthropogenic enhancements to production of highly oxygenated molecules from autoxidation, Proc. Natl. Acad. Sci. U. S. A., 116, 6641-6646, 10.1073/pnas.1810774116, 2019.

Qi, X. M., Ding, A. J., Nie, W., Petäjä, T., Kerminen, V. M., Herrmann, E., Xie, Y. N., Zheng, L. F., Manninen, H., Aalto, P., Sun, J. N., Xu, Z. N., Chi, X. G., Huang, X., Boy, M., Virkkula, A., Yang, X. Q., Fu, C. B., and Kulmala, M.: Aerosol size distribution and new particle formation in the western Yangtze River Delta of China: 2 years of measurements at the SORPES station, Atmospheric Chemistry and Physics, 15, 12445-12464, 10.5194/acp-15-12445-2015, 2015.

Riccobono, F., Schobesberger, S., Scott, C. E., Dommen, J., Ortega, I. K., Rondo, L., Almeida, J., Amorim, A., Bianchi, F., Breitenlechner, M., David, A., Downard, A., Dunne, E. M., Duplissy, J., Ehrhart, S., Flagan, R. C., Franchin, A., Hansel, A., Junninen, H., Kajos, M., Keskinen, H., Kupc, A., Kuerten, A., Kvashin, A. N., Laaksonen, A., Lehtipalo, K., Makhmutov, V., Mathot, S., Nieminen, T., Onnela, A., Petaja, T., Praplan, A. P., Santos, F. D., Schallhart, S., Seinfeld, J. H., Sipila, M., Spracklen, D. V., Stozhkov, Y., Stratmann, F., Tome, A., Tsagkogeorgas, G., Vaattovaara, P., Viisanen, Y., Vrtala, A., Wagner, P. E., Weingartner, E., Wex, H., Wimmer, D., Carslaw, K. S., Curtius, J., Donahue, N. M., Kirkby, J., Kulmala, M., Worsnop, D. R., and Baltensperger, U.: Oxidation products of biogenic emissions contribute to nucleation of atmospheric particles, Science, 344, 717-721, 10.1126/science.1243527, 2014.

Richters, S., Herrmann, H., and Berndt, T.: Highly oxidized RO_2 radicals and consecutive products from the ozonolysis of three sesquiterpenes, Environmental Science & Technology, 50, 2354-2362, 10.1021/acs.est.5b05321, 2016.

Rippen, G., Zietz, E., Frank, R., Knacker, T., and Klöpffer, W.: Do airborne nitrophenols contribute to forest decline?, Environmental Technology Letters, 8, 475-482, 10.1080/09593338709384508, 1987.

Rollins, A. W., Browne, E. C., Min, K. E., Pusede, S. E., Wooldridge, P. J., Gentner, D. R., Goldstein, A. H., Liu, S., Day, D. A., Russell, L. M., and Cohen, R. C.: Evidence for NO_x control over nighttime SOA formation, Science, 337, 1210, 10.1126/science.1221520, 2012.

Shen, Y., Virkkula, A., Ding, A., Wang, J., Chi, X., Nie, W., Qi, X., Huang, X., Liu, Q., Zheng, L., Xu, Z., Petäjä, T., Aalto, P. P., Fu, C., and Kulmala, M.: Aerosol optical properties at SORPES in Nanjing, east China, Atmospheric Chemistry and Physics, 18, 5265-5292, 10.5194/acp-18-5265-2018, 2018.

Sindelarova, K., Granier, C., Bouarar, I., Guenther, A., Tilmes, S., Stavrakou, T., Müller, J. F., Kuhn, U., Stefani, P., and Knorr, W.: Global data set of biogenic VOC emissions calculated by the MEGAN model over the last 30 years, Atmospheric Chemistry and Physics, 14, 9317-9341, 10.5194/acp-14-9317-2014, 2014.

Stolzenburg, D., Fischer, L., Vogel, A. L., Heinritzi, M., Schervish, M., Simon, M., Wagner, A. C., Dada, L., Ahonen, L. R., Amorim, A., Baccarini, A., Bauer, P. S., Baumgartner, B., Bergen, A., Bianchi, F., Breitenlechner, M., Brilke, S., Mazon, S. B., Chen, D., Dias, A., Draper, D. C., Duplissy, J., El Haddad, I., Finkenzeller, H., Frege, C., Fuchs, C., Garmash, O., Gordon, H., He, X., Helm, J., Hofbauer, V., Hoyle, C. R., Kim, C., Kirkby, J., Kontkanen, J., Kuerten, A., Lampilahti, J., Lawler, M., Lehtipalo, K., Leiminger, M., Mai, H., Mathot, S., Mentler, B., Molteni, U., Nie, W., Nieminen, T., Nowak, J. B., Ojdanic, A., Onnela, A., Passananti, M., Petaja, T., Quelever, L. L. J., Rissanen, M. P., Sarnela, N., Schallhart, S., Tauber, C., Tome, A., Wagner, R., Wang, M., Weitz, L., Wimmer, D., Xiao, M., Yan, C., Ye, P., Zha, Q., Baltensperger, U., Curtius, J., Dommen, J., Flagan, R. C., Kulmala, M., Smith, J. N., Worsnop, D. R., Hansel, A., Donahue, N. M., and Winkler, P. M.: Rapid growth of organic aerosol nanoparticles over a wide tropospheric temperature range, Proc. Natl. Acad. Sci. U. S. A., 115, 9122-9127, 10.1073/pnas.1807604115, 2018.

Sun, P., Nie, W., Chi, X., Xie, Y., Huang, X., Xu, Z., Qi, X., Xu, Z., Wang, L., Wang, T., Zhang, Q., and Ding, A.: Two years of online measurement of fine particulate nitrate in the western Yangtze River Delta: influences of thermodynamics and N_2O_5 hydrolysis, Atmospheric Chemistry and Physics, 18, 17177-

17190, 10.5194/acp-18-17177-2018, 2018.

Sun, P., Nie, W., Wang, T., Chi, X., Huang, X., Xu, Z., Zhu, C., Wang, L., Qi, X., Zhang, Q., and Ding, A.: Impact of air transport and secondary formation on haze pollution in the Yangtze River Delta: In situ online observations in Shanghai and Nanjing, Atmos. Environ., 225, 117350, https://doi.org/10.1016/j.atmosenv.2020.117350, 2020.

Takeuchi, M., and Ng, N. L.: Chemical composition and hydrolysis of organic nitrate aerosol formed from hydroxyl and nitrate radical oxidation of α-pinene and β-pinene, Atmos. Chem. Phys., 19, 12749-12766, 10.5194/acp-19-12749-2019, 2019.

Trostl, J., Chuang, W. K., Gordon, H., Heinritzi, M., Yan, C., Molteni, U., Ahlm, L., Frege, C., Bianchi, F., Wagner, R., Simon, M., Lehtipalo, K., Williamson, C., Craven, J. S., Duplissy, J., Adamov, A., Almeida, J., Bernhammer, A. K., Breitenlechner, M., Brilke, S., Dias, A., Ehrhart, S., Flagan, R. C., Franchin, A., Fuchs, C., Guida, R., Gysel, M., Hansel, A., Hoyle, C. R., Jokinen, T., Junninen, H., Kangasluoma, J., Keskinen, H., Kim, J., Krapf, M., Kurten, A., Laaksonen, A., Lawler, M., Leiminger, M., Mathot, S., Mohler, O., Nieminen, T., Onnela, A., Petaja, T., Piel, F. M., Miettinen, P., Rissanen, M. P., Rondo, L., Sarnela, N., Schobesberger, S., Sengupta, K., Sipila, M., Smith, J. N., Steiner, G., Tome, A., Virtanen, A., Wagner, A. C., Weingartner, E., Wimmer, D., Winkler, P. M., Ye, P., Carslaw, K. S., Curtius, J., Dommen, J., Kirkby, J., Kulmala, M., Riipinen, I., Worsnop, D. R., Donahue, N. M., and Baltensperger, U.: The role of low-volatility organic compounds in initial particle growth in the atmosphere, Nature, 533, 527-531, 10.1038/nature18271, 2016.

Tsiligiannis, E., Hammes, J., Salvador, C. M., Mentel, T. F., and Hallquist, M.: Effect of NO_x on 1,3,5-trimethylbenzene (TMB) oxidation product distribution and particle formation, Atmospheric Chemistry and Physics, 19, 15073-15086, 10.5194/acp-19-15073-2019, 2019.

Wang, J., Nie, W., Cheng, Y., Shen, Y., Chi, X., Wang, J., Huang, X., Xie, Y., Sun, P., Xu, Z., Qi, X., Su, H., and Ding, A.: Light absorption of brown carbon in eastern China based on 3-year multi-wavelength aerosol optical property observations and an improved absorption Ångström exponent segregation method, Atmos. Chem. Phys., 18, 9061-9074, 10.5194/acp-18-9061-2018, 2018a.

Wang, J., Feng, L., Palmer, P. I., Liu, Y., Fang, S., Bosch, H., O'Dell, C. W., Tang, X., Yang, D., Liu, L., and Xia, C.: Large Chinese land carbon sink estimated from atmospheric carbon dioxide data, Nature, 586, 720-723, 10.1038/s41586-020-2849-9, 2020a.

Wang, L., Wang, X., Gu, R., Wang, H., Yao, L., Wen, L., Zhu, F., Wang, W., Xue, L., Yang, L., Lu, K., Chen, J., Wang, T., Zhang, Y., and Wang, W.: Observations of fine particulate nitrated phenols in four sites in northern China: concentrations, source apportionment, and secondary formation, Atmospheric Chemistry and Physics, 18, 4349-4359, 10.5194/acp-18-4349-2018, 2018b.

Wang, M., Chen, D., Xiao, M., Ye, Q., Stolzenburg, D., Hofbauer, V., Ye, P., Vogel, A. L., Mauldin, R. L., Amorim, A., Baccarini, A., Baumgartner, B., Brilke, S., Dada, L., Dias, A., Duplissy, J., Finkenzeller, H., Garmash, O., He, X.-C., Hoyle, C. R., Kim, C., Kvashnin, A., Lehtipalo, K., Fischer, L., Molteni, U., Petäjä, T., Pospisilova, V., Quéléver, L. L. J., Rissanen, M., Simon, M., Tauber, C., Tomé, A., Wagner, A. C., Weitz, L., Volkamer, R., Winkler, P. M., Kirkby, J., Worsnop, D. R., Kulmala, M., Baltensperger, U., Dommen, J., El-Haddad, I., and Donahue, N. M.: Photo-oxidation of aromatic hydrocarbons produces low-volatility organic compounds, Environmental Science & Technology, 54, 7911-7921, 10.1021/acs.est.0c02100, 2020b.

Wang, S., Wu, R., Berndt, T., Ehn, M., and Wang, L.: Formation of Highly Oxidized Radicals and Multifunctional Products from the Atmospheric Oxidation of Alkylbenzenes, Environ Sci Technol, 51, 8442-8449, 10.1021/acs.est.7b02374, 2017.

Wang, Y., Mehra, A., Krechmer, J. E., Yang, G., Hu, X., Lu, Y., Lambe, A., Canagaratna, M., Chen, J., Worsnop, D., Coe, H., and Wang, L.: Oxygenated products formed from OH-initiated reactions of trimethylbenzene: autoxidation and accretion, Atmospheric Chemistry and Physics, 20, 9563-9579, 10.5194/acp-20-9563-2020, 2020c.

Wang, Z., Ehn, M., Rissanen, M. P., Garmash, O., Quéléver, L., Xing, L., Monge-Palacios, M., Rantala, P., Donahue, N. M., Berndt, T., and Sarathy, S. M.: Efficient alkane oxidation under combustion engine and atmospheric conditions, Communications Chemistry, 4, 18, 10.1038/s42004-020-00445-3, 2021.

Wayne, R. P., Barnes, I., Biggs, P., Burrows, J. P., Canosamas, C. E., Hjorth, J., Lebras, G., Moortgat, G. K., Perner, D., Poulet, G., Restelli, G., and Sidebottom, H.: The nitrated radical - physics, chemistry, and the atmosphere, Atmospheric Environment Part a-General Topics, 25, 1-203, 10.1016/0960-1686(91)90192-a, 1991.

Wennberg, P. O., Bates, K. H., Crounse, J. D., Dodson, L. G., McVay, R. C., Mertens, L. A., Nguyen, T. B., Praske, E., Schwantes, R. H., Smarte, M. D., St Clair, J. M., Teng, A. P., Zhang, X., and Seinfeld, J. H.: Gas-phase reactions of isoprene and its major oxidation products, Chem Rev, 118, 3337-3390, 10.1021/acs.chemrev.7b00439, 2018.

Wood, E. C., Canagaratna, M. R., Herndon, S. C., Onasch, T. B., Kolb, C. E., Worsnop, D. R., Kroll, J. H., Knighton, W. B., Seila, R., Zavala, M., Molina, L. T., DeCarlo, P. F., Jimenez, J. L., Weinheimer, A. J., Knapp, D. J., Jobson, B. T., Stutz, J., Kuster, W. C., and Williams, E. J.: Investigation of the correlation between odd oxygen and secondary organic aerosol in Mexico City and Houston, Atmospheric Chemistry and Physics, 10, 8947-8968, 10.5194/acp-10-8947-2010, 2010.

Xia, M., Peng, X., Wang, W., Yu, C., Sun, P., Li, Y., Liu, Y., Xu, Z., Wang, Z., Xu, Z., Nie, W., Ding, A., and Wang, T.: Significant production of $ClNO_2$ and possible source of Cl_2 from N_2O_5 uptake at a suburban site in eastern China, Atmos. Chem. Phys., 20, 6147-6158, 10.5194/acp-20-6147-2020, 2020.

Xie, Y., Ding, A., Nie, W., Mao, H., Qi, X., Huang, X., Xu, Z., Kerminen, V.-M., Petäjä, T., Chi, X., Virkkula, A., Boy, M., Xue, L., Guo, J., Sun, J., Yang, X., Kulmala, M., and Fu, C.: Enhanced sulfate formation by nitrogen dioxide: Implications from in situ observations at the SORPES station, Journal of Geophysical Research: Atmospheres, 120, 12679-12694, 10.1002/2015jd023607, 2015.

Xiong, F., McAvey, K. M., Pratt, K. A., Groff, C. J., Hostetler, M. A., Lipton, M. A., Starn, T. K., Seeley, J. V., Bertman, S. B., Teng, A. P., Crounse, J. D., Nguyen, T. B., Wennberg, P. O., Misztal, P. K., Goldstein, A. H., Guenther, A. B., Koss, A. R., Olson, K. F., de Gouw, J. A., Baumann, K., Edgerton, E. S., Feiner, P. A., Zhang, L., Miller, D. O., Brune, W. H., and Shepson, P. B.: Observation of isoprene hydroxynitrates in the southeastern United States and implications for the fate of NO_x, Atmos. Chem. Phys., 15, 11257-11272, 10.5194/acp-15-11257-2015, 2015.

Xu, Z., Huang, X., Nie, W., Chi, X., Xu, Z., Zheng, L., Sun, P., and Ding, A.: Influence of synoptic condition and holiday effects on VOCs and ozone production in the Yangtze River Delta region, China, Atmos. Environ., 168, 112-124, 10.1016/j.atmosenv.2017.08.035, 2017.

Xu, Z., Huang, X., Nie, W., Shen, Y., Zheng, L., Xie, Y., Wang, T., Ding, K., Liu, L., Zhou, D., Qi, X., and Ding, A.: Impact of biomass burning and vertical mixing of residual-layer aged plumes on ozone in the Yangtze River Delta, China: a tethered-balloon measurement and modeling study of a multiday ozone opisode, Journal of Geophysical Research: Atmospheres, 123, 11,786-711,803, 10.1029/2018jd028994, 2018.

Xu, Z. N., Nie, W., Liu, Y. L., Sun, P., Huang, D. D., Yan, C., Krechmer, J., Ye, P. L., Xu, Z., Qi, X. M., Zhu, C. J., Li, Y. Y., Wang, T. Y., Wang, L., Huang, X., Tang, R. Z., Guo, S., Xiu, G. L., Fu, Q. Y., Worsnop, D., Chi, X. G., and Ding, A. J.: Multifunctional products of isoprene oxidation in polluted

atmosphere and their contribution to SOA, Geophysical Research Letters, 48, 10.1029/2020gl089276, 2021.

Yan, C., Nie, W., Äijälä, M., Rissanen, M. P., Canagaratna, M. R., Massoli, P., Junninen, H., Jokinen, T., Sarnela, N., Häme, S. A. K., Schobesberger, S., Canonaco, F., Yao, L., Prévôt, A. S. H., Petäjä, T., Kulmala, M., Sipilä, M., Worsnop, D. R., and Ehn, M.: Source characterization of highly oxidized multifunctional compounds in a boreal forest environment using positive matrix factorization, Atmospheric Chemistry and Physics, 16, 12715-12731, 10.5194/acp-16-12715-2016, 2016.

Yan, C., Nie, W., Vogel, A. L., Dada, L., Lehtipalo, K., Stolzenburg, D., Wagner, R., Rissanen, M. P., Xiao, M., Ahonen, L., Fischer, L., Rose, C., Bianchi, F., Gordon, H., Simon, M., Heinritzi, M., Garmash, O., Roldin, P., Dias, A., Ye, P., Hofbauer, V., Amorim, A., Bauer, P. S., Bergen, A., Bernhammer, A. K., Breitenlechner, M., Brilke, S., Buchholz, A., Mazon, S. B., Canagaratna, M. R., Chen, X., Ding, A., Dommen, J., Draper, D. C., Duplissy, J., Frege, C., Heyn, C., Guida, R., Hakala, J., Heikkinen, L., Hoyle, C. R., Jokinen, T., Kangasluoma, J., Kirkby, J., Kontkanen, J., Kürten, A., Lawler, M. J., Mai, H., Mathot, S., Mauldin, R. L., Molteni, U., Nichman, L., Nieminen, T., Nowak, J., Ojdanic, A., Onnela, A., Pajunoja, A., Petäjä, T., Piel, F., Quéléver, L. L. J., Sarnela, N., Schallhart, S., Sengupta, K., Sipilä, M., Tomé, A., Tröstl, J., Väisänen, O., Wagner, A. C., Ylisirniö, A., Zha, Q., Baltensperger, U., Carslaw, K. S., Curtius, J., Flagan, R. C., Hansel, A., Riipinen, I., Smith, J. N., Virtanen, A., Winkler, P. M., Donahue, N. M., Kerminen, V. M., Kulmala, M., Ehn, M., and Worsnop, D. R.: Size-dependent influence of NO_x on the growth rates of organic aerosol particles, Science Advances, 6, eaay4945, 10.1126/sciadv.aay4945, 2020.

Yang, L., Nie, W., Liu, Y., Xu, Z., Xiao, M., Qi, X., Li, Y., Wang, R., Zou, J., Paasonen, P., Yan, C., Xu, Z., Wang, J., Zhou, C., Yuan, J., Sun, J., Chi, X., Kerminen, V.-M., Kulmala, M., and Ding, A.: Towards building a physical proxy for gas-phase sulfuric acid concentration based on its budget analysis in polluted Yangtze River Delta, east China, Environmental Science & Technology, https://doi.org/10.1021/acs.est.1c00738, 2021.

Yuan, B., Liggio, J., Wentzell, J., Li, S.-M., Stark, H., Roberts, J. M., Gilman, J., Lerner, B., Warneke, C., Li, R., Leithead, A., Osthoff, H. D., Wild, R., Brown, S. S., and de Gouw, J. A.: Secondary formation of nitrated phenols: insights from observations during the Uintah Basin Winter Ozone Study (UBWOS) 2014, Atmospheric Chemistry and Physics, 16, 2139-2153, 10.5194/acp-16-2139-2016, 2016.

Zaytsev, A., Koss, A. R., Breitenlechner, M., Krechmer, J. E., Nihill, K. J., Lim, C. Y., Rowe, J. C., Cox, J. L., Moss, J., Roscioli, J. R., Canagaratna, M. R., Worsnop, D. R., Kroll, J. H., and Keutsch, F. N.: Mechanistic study of the formation of ring-retaining and ring-opening products from the oxidation of aromatic compounds under urban atmospheric conditions, Atmospheric Chemistry and Physics, 19, 15117-15129, 10.5194/acp-19-15117-2019, 2019.

Zhang, Q., Jimenez, J. L., Canagaratna, M. R., Allan, J. D., Coe, H., Ulbrich, I., Alfarra, M. R., Takami, A., Middlebrook, A. M., Sun, Y. L., Dzepina, K., Dunlea, E., Docherty, K., DeCarlo, P. F., Salcedo, D., Onasch, T., Jayne, J. T., Miyoshi, T., Shimono, A., Hatakeyama, S., Takegawa, N., Kondo, Y., Schneider, J., Drewnick, F., Borrmann, S., Weimer, S., Demerjian, K., Williams, P., Bower, K., Bahreini, R., Cottrell, L., Griffin, R. J., Rautiainen, J., Sun, J. Y., Zhang, Y. M., and Worsnop, D. R.: Ubiquity and dominance of oxygenated species in organic aerosols in anthropogenically-influenced Northern Hemisphere midlatitudes, Geophysical Research Letters, 34, 6, 10.1029/2007gl029979, 2007.

Zhang, Y., Tang, L., Croteau, P. L., Favez, O., Sun, Y., Canagaratna, M. R., Wang, Z., Couvidat, F., Albinet, A., Zhang, H., Sciare, J., Prévôt, A. S. H., Jayne, J. T., and Worsnop, D. R.: Field characterization of the $PM_{2.5}$ Aerosol Chemical Speciation Monitor: insights into the composition, sources, and processes of fine particles in eastern China, Atmos. Chem. Phys., 17, 14501-14517, 10.5194/acp-17-14501-2017,

1386 2017.

1387 Zhang, Y., Peräkylä, O., Yan, C., Heikkinen, L., Äijälä, M., Daellenbach, K. R., Zha, Q., Riva, M.,
1388 Garmash, O., Junninen, H., Paatero, P., Worsnop, D., and Ehn, M.: A novel approach for simple statistical
1389 analysis of high-resolution mass spectra, Atmos. Meas. Tech., 12, 3761-3776, 10.5194/amt-12-3761-
1390 2019, 2019.

1391 Zhang, Y., Peräkylä, O., Yan, C., Heikkinen, L., Äijälä, M., Daellenbach, K. R., Zha, Q., Riva, M.,
1392 Garmash, O., Junninen, H., Paatero, P., Worsnop, D., and Ehn, M.: Insights into atmospheric oxidation
1393 processes by performing factor analyses on subranges of mass spectra, Atmos. Chem. Phys., 20, 5945-
1394 5961, 10.5194/acp-20-5945-2020, 2020.

1395 Zhao, D., Pullinen, I., Fuchs, H., Schrade, S., Wu, R., Acir, I. H., Tillmann, R., Rohrer, F., Wildt, J., Guo,
1396 Y., Kiendler-Scharr, A., Wahner, A., Kang, S., Vereecken, L., and Mentel, T. F.: Highly oxygenated
1397 organic molecules (HOM) formation in the isoprene oxidation by NO_3 radical, Atmos. Chem. Phys.
1398 Discuss., 2020, 1-28, 10.5194/acp-2020-1178, 2020.

1399 Ziemann, P. J., and Atkinson, R.: Kinetics, products, and mechanisms of secondary organic aerosol
1400 formation, Chemical Society Reviews, 41, 6582-6605, 10.1039/c2cs35122f, 2012.

1401